Published in final edited form as:

Science. 2023 March 31; 379(6639): eabm5658. doi:10.1126/science.abm5658.

Multimodal control of dendritic cell functions by nociceptors

Pavel Hanč[1,2], **Rodrigo J. Gonzalez**[1,2], **Irina B. Mazo**[1,2], **Yidi Wang**[1,2], **Talley Lambert**[3], **Gloria Ortiz**[4], **Evan W. Miller**[4], **Ulrich H. von Andrian**[1,2]

[1]Department of Immunology, Harvard Medical School; Boston, MA 02115, USA

[2]The Ragon Institute of MGH, MIT and Harvard; Cambridge, MA 02139, USA

[3]Cell Biology Microscopy Facility, Harvard Medical School; Boston, MA 02115, USA

[4]Departments of Chemistry, Molecular & Cell Biology, and Helen Wills Neuroscience Institute. University of California; Berkeley, CA 94720, USA.

Abstract

Interactions between nociceptors and dendritic cells (DCs) can modulate immune responses in barrier tissues. Our understanding of the underlying communication frameworks remains rudimentary however. Here, we show that nociceptors control DCs in three molecularly distinct ways. First, nociceptors release calcitonin gene-related peptide (CGRP), which imparts a distinct transcriptional profile on steady-state DCs characterized by expression of pro-IF-1β and other genes implicated in DC sentinel functions. Second, nociceptor activation induces contact-dependent calcium fluxes and membrane depolarization in DCs and enhances their production of proinflammatory cytokines when stimulated. Finally, nociceptor-derived chemokine CCL2 contributes to the orchestration of DC-dependent local inflammation as well as induction of adaptive responses against skin-acquired antigens. Thus, the combined actions of nociceptor-derived chemokines, neuropeptides, and electrical activity fine-tune DC responses in barrier tissues.

One-sentence summary:

Nociceptors control dendritic cell functions in a context-dependent manner by secreting the chemokine CCL2, through their electrical activity requiring direct cell-to-cell contact, and by means of releasing the neuropeptide CGRP.

Nociceptors are sensory neurons that respond to noxious stimuli by eliciting sensations of pain or itch, and by modulating immune responses (1-4). Their somata reside in dorsal root ganglia (DRGs) with axons projecting to both the spinal cord and peripheral

---

Author contributions: P.H. and U.H.v.A. conceived the study, interpreted results, and wrote the manuscript. P.H. performed experiments and analyzed data. R.J.G. performed intradermal injections. I.B.M. generated bone marrow chimeras and performed CHS experiments. Y.W. prepared cortical and hippocampal neuronal cultures. T.L. performed light sheet microscopy imaging. G.O. and E.W.M. generated the voltage-sensitive dye BeRST.

Competing interests: U.H.v.A. is a paid consultant with financial interest of Avenge Bio, Beam Therapeutics, Bluesphere Bio, Curon, DNAlite, Gate Biosciences, Gentibio, Intergalactic, intrECate Biotherapeutics, Interon, Mallinckrodt Pharmaceuticals, Moderna, Monopteros Biotherapeutics, Morphic Therapeutics, Rubius, Selecta and SQZ. E.W.M. is an inventor on a patent describing BeRST - WO2017019908. All other authors declare that they have no competing interests.

tissues (5). Nociceptors densely innervate barrier tissues (6), such as the skin and mucosal surfaces, which are also populated by dendritic cells (DCs). These sentinel leukocytes sense pathogen- and danger-associated molecular patterns and play critical roles in antigen presentation and control of adaptive immunity. Moreover, DCs coordinate local inflammation by secreting cytokines and other mediators (7). Intravital imaging demonstrated that dermal DCs congregate tightly around nociceptors, which profoundly impact DC functions (8-10). However, although these observations suggest direct cell–cell communication, the requirement for physical DC–nociceptor interactions versus a possible involvement of other intermediary cells has not been established. Furthermore, the role of nociceptor-derived neuropeptides in DC–nociceptor communication has been controversial, as neuropeptides appear dispensable in some experimental settings but exert either pro- or anti-inflammatory effects in other models (8, 9, 11).

Nociceptors potentiate cytokine responses by DC in vitro

To address these outstanding questions, we cocultured primary DRG neurons and Flt3L-induced bone marrow (BM) DCs (fig. S1A). Neuronal cultures contained >90% small-diameter $NaV1.8^+$ nociceptors (fig. S1B), whereas BMDC cultures comprised three major subsets: type 1 and 2 conventional DCs (cDCs) and plasmacytoid DCs (pDCs) (fig. S1C). Using this system, we examined DC responses to a TLR7 agonist, imiquimod (IMQ). Nociceptors did not impact DC maturation marker expression upon IMQ treatment (fig. S2A), but their presence significantly enhanced DC production of IL-12 p40—the shared subunit of IL-12 and IL-23 (Fig. 1A)—as well as IL-6 (Fig. 1B). Conversely, production of another proinflammatory cytokine, TNFα, was reduced (Fig. 1C). A likely mechanism for TNFα downregulation is the action of calcitonin gene-related peptide (CGRP), a nociceptor-derived neuropeptide known to inhibit cytokine production by myeloid leukocytes (11). Indeed, olcegepant, a CGRP receptor antagonist, rescued TNFα production in DC–nociceptor cocultures, but had no impact on DCs alone (fig. S2B). Olcegepant did not affect DC production of IL-12 p40 or IL-6 regardless of whether nociceptors were present or not (fig. S2, C and D), indicating that this cytokine-promoting effect of nociceptors on DCs was CGRP-independent. By contrast, a different myeloid cell type (BM-derived macrophages) showed decreased or unaltered cytokine responses to IMQ in nociceptor cocultures (Fig. 1D). Finally, coculture with hippocampal or cortical neurons did not alter DC responses to IMQ (Fig. 1E and fig. S2E). Thus, the potentiation of inflammatory cytokine production (other than TNFα) is a unique and specific consequence of the DC–nociceptor dialogue.

Numerous stimuli can trigger inflammatory cytokine production by DCs, including damage-associated molecular patterns (DAMPs) released from dead or distressed cells (12). A DC response to DAMPs from dead nociceptors could conceivably provide a trivial explanation for the exacerbated IMQ effect. However, DCs cocultured with nociceptors killed by prior fixation showed no enhanced cytokine production (Fig. 1F and fig. S2F). Moreover, treatment with lidocaine (a voltage-gated sodium channel blocker) and QX314 (a membrane-impermeable quaternary derivative of lidocaine), which together produce a long-lasting blockade of neuronal activity (13), dampened the ability of nociceptors to

potentiate DC cytokine responses (Fig. 1G and fig. S2G). Thus, nociceptors must be alive and electrically active to exert their effects.

IMQ stimulated IL-12 p40 production only in a fraction of DCs, which increased in a concentration-dependent manner. Nociceptor cocultures increased the frequency of responding cDCs, but did not grossly alter the amount of cytokine detected per cell (Fig. 1H). By contrast, IMQ treatment of pDCs induced only a modest response, which was minimally affected by nociceptors (fig. S3A). Accordingly, the accumulation of IFNβ—a prototypical pDC cytokine (14)—was also unaffected by nociceptors (fig. S3B). Finally, although only cDC2s and pDCs produced IL-6 in response to IMQ (fig. S3C), the proportion of IL-6^+ cDC2s was significantly increased in the presence of nociceptors (fig. S3C), whereas pDCs in nociceptor cocultures showed only a weak, statistically non-significant trend toward increased IL-6 production (fig. S3C). Thus, cDCs, but not pDCs, are impacted by nociceptors, at least under these experimental conditions, and the presence of electrically active nociceptors increases the proportion of DCs responding to a given dose of IMQ, presumably by decreasing the activation threshold to initiate cytokine production.

Cytokine potentiation requires concomitant activation of nociceptors and DCs.

The principal IMQ receptor, TLR7 (15), is robustly expressed in murine DCs but has also been reported in sensory neurons (16). To clarify its role in this process, we established cocultures in which either nociceptors or DCs had been harvested from *Tlr7*$^{-/-}$ mice (17). Cytokine responses to IMQ were abrogated when DCs lacked TLR7, whereas *Tlr7*$^{-/-}$ and WT nociceptors equally enhanced cytokine production by WT DCs (Fig. 1I and fig. S4A). Thus, nociceptors cannot by themselves elicit a cytokine response in DCs unless DCs are directly stimulated. Nonetheless, concomitant IMQ stimulation of nociceptors was required, albeit independently of TLR7. IMQ can directly gate the cation channel TRPA1 (18, 19) and a TRPA1 inhibitor prevented nociceptor enhancement of DC responses to IMQ (fig. S4B).

That IMQ may act on both DCs and nociceptors, albeit through different mechanisms, prompted us to investigate other immune stimuli, including zymosan (TLR2 and Dectin-1 agonist), polyinosinic: polycytidylie acid (poly-I:C) (TLR3 agonist), lipopolysaccharide (LPS) (TLR4 agonist), flagellin (TLR5 agonist), or CpG (TLR9 agonist). All of these agents activate DCs, but only LPS, flagellin, and zymosan stimulate nociceptors by direct gating of ion channels or through membrane receptors such as TLR4 or Dectin-1 (20-22). Accordingly, nociceptors potentiated DC cytokine responses to zymosan, LPS, and flagellin, but not to poly-I:C or CpG (Fig. 2A and fig. S4C). Finally, as expected, nociceptors potentiated the LPS response irrespective of TLR7 expression by DCs (fig. S4D), indicating that *Tlr7*$^{-/-}$ DCs did not respond to IMQ because of their inability to register the stimulus and not due to other inherent functional defects.

Next, to test whether nociceptors can also enhance DC cytokine responses to infectious microbes, we exposed nociceptor-DC cocultures to viral (influenza A virus (IAV)), bacterial (UV-inactivated *Streptococcus pnneumoniae*), or fungal (*Candida albicans*) pathogens that are commonly encountered in barrier tissues. IL-12 p40 was induced by every tested

pathogen, whereas IL-6 only by *S. pneumoniae* and IAV. Regardless of the microbial challenge, coculture with nociceptors markedly enhanced these responses (Fig. 2B and fig. S4E), suggesting that the paradigm of nociceptor enhancement of DC cytokine production may apply to a host of inflammatory and infectious stimuli.

DC cytokine potentiation by nociceptors requires physical contact but not neuropeptides.

Upon activation, nociceptors release immunomodulatory neuropeptides, particularly the CGRP-family of neuropeptides (CGRP, adrenomedullin, and intermedin) (23), substance P (SP) (24), vasoactive intestinal peptide (VIP) (25), and pituitary adenylate cyclase-activating peptide (PACAP) (25). However, DC exposure to neuropeptides did not enhance IMQ induced production of IL-12 p40 or IL-6, nor did neuropeptides induce de novo cytokine responses in unstimulated DCs (fig. S4F). Similarly, nociceptor-conditioned medium did not enhance cytokine production by IMQ-stimulated DCs, suggesting that direct cell–cell contact may be required (Fig. 2C and fig. S4G). Indeed, when DCs and nociceptors were separated by a filter membrane in a Transwell device that allowed diffusion of soluble molecules while preventing physical contact, DCs produced no more IL-12 p40 than DCs cultured alone (Fig. 2D). Furthermore, the accumulation of IL-6 was decreased, albeit not quite to the levels observed in DC-only cultures (fig. S4H). Thus the presence of electrically competent nociceptors enhances DC cytokine responses to multiple exogenous immune stimuli in a manner independent of neuropeptides and dependent on physical contact or, at least, close physical proximity.

Nociceptors attract DCs by secreting CCL2

Seeing the importance of physical contact for nociceptor–DC communication in vitro, and in light of their close proximity in vivo (9, 10), we asked if nociceptors produce DC chemoattractants. Indeed, all DC subsets migrated toward nociceptor-conditioned medium in a concentration-dependent manner (Fig. 3A and fig. S5, A and B). Using two multiplexed assays, we identified several known chemoattractants in nociceptor-conditioned media, with CCL2 and chemerin being the most abundant (fig. S5, C and D). Although chemerin immunodepletion had no effect, CCL2 depletion significantly decreased DC migration toward nociceptor-conditioned medium (fig. S5E). Furthermore, medium conditioned by nociceptors from *Ccl2*$^{-/-}$ mice (26) showed a reduced capacity to attract DCs (Fig. 3A and fig. S5, A and B), indicating that CCL2 is the predominant DC chemoattractant secreted by nociceptors. Accordingly, CCL2 was detectable in media conditioned by WT but not *Ccl2*$^{-/-}$ nociceptors (fig. S5F) and increased after nociceptor stimulation with capsaicin or IMQ (fig. S5G). A previous report linked CCL2 upregulation in nociceptors to activation of MyD88, a signaling adaptor critical for TLR function (27). Indeed, LPS-induced ligation of TLR4, resulted in markedly increased levels of CCL2 (fig. S5H). Moreover, in agreement with previous studies, unstimulated cDC1s and cDC2s expressed uniformly high levels of the CCL2 receptor, CCR2, which was downregulated upon LPS exposure, coincident with CCR7 upregulation (fig. S5I) (28). In macrophages, CCL2 reportedly impacts the secretion

of cytokines including IL-12 (29). However, CCL2 had no effect on cytokine production by DCs, as *Ccl2*$^{-/-}$ and WT nociceptors potentiated the DC response to IMQ equally (fig. S5J).

DCs engage in tight and dynamic interactions with nociceptors

Next, using live-cell imaging, we observed that DCs engaged in tight and highly dynamic physical interactions with nociceptors (Fig. 3B; fig. S6A; and movies S1 to S3). Furthermore, transmission electron microscopy revealed a tight apposition of the plasma membranes of interacting cells (Fig. 3C). To ask if similarly tight contacts occur in vivo, we transplanted BM from *Zbtb46*^{eGFP} donors (30) into irradiated *Scnl0a*$^{Cre/+}$ *Rosa26*$^{tdTomato/+}$ recipients. Nociceptors and DCs in these chimeras were identifiable by expression of tdTomato and GFP, respectively, and confocal microscopy analysis of dermal sheets revealed physical contacts between them (Fig. 3D).

Nociceptor activation induces calcium flux in interacting DCs

Given the importance of physical contact for effective communication between nociceptors and DCs and the observation that nociceptors attract DCs by secretion of CCL2, we performed calcium imaging to assess whether and how signals propagate from activated neurons to interacting DCs. Upon treatment with a TRPV1 channel agonist, capsaicin (31), a rapid increase in intracellular calcium occurred in both nociceptors and DCs (Fig. 4, A and B, and movie S4). Capsaicin did not elicit a calcium flux in DCs alone (Fig. 4B and movie S5), indicating that the capsaicin effect in cocultures was due to activation of nociceptors, not DCs.

To better approximate the anatomic relationship between DCs and nociceptors, we next employed a culture device with two compartments connected by fluidically isolated microgrooves (32) (fig. S6B). Nociceptors plated in one compartment (“neuronal compartment”) sprouted axons across the microgrooves into the second compartment (“DC compartment”). Capsaicin stimulation of nociceptors in the neuronal compartment triggered axonal action potential propagation to the DC compartment, where DCs interacting with firing axonal segments fluxed calcium (Fig. 4C and movie S6) comparably to conventional cocultures (fig. S6C). Although some DCs fluxed calcium in sync with contacting axons (fig. S6D and movie S7), calcium flux kinetics in the DC population as a whole were nonuniform (Fig. 4C and fig. S6E), a phenomenon likely attributable to the dynamic nature of interactions, asynchronous firing of different axons, non-homogeneous distribution of TRPV-1 expression among nociceptors, and potentially also differences between DC subsets.

Nociceptor activation induces membrane depolarization in interacting DCs

Neuronal calcium influx is triggered by membrane depolarization as action potentials propagate along axons. Consequently, we wondered if the calcium flux in DCs was also accompanied by membrane depolarization. Indeed, using a ratiometric fluorescent probe, Di-8-ANNEPS, capsaicin-induced membrane depolarization was detected in both cell types in DC–nociceptor cocultures. Capsaicin, however, had no effect on DCs alone (fig. S6F and

movies S8 and S9). Similarly, DCs and nociceptors stained with BeRST, a voltage-sensitive dye compatible with calcium imaging (33), depolarized and fluxed calcium in response to capsaicin (Fig. 4D and movie S10).

Thus, nociceptors attract DCs by producing CCL2 and engage in tight physical interactions, presumably mediated by yet-to-be-identified adhesion molecule(s). Electrical nociceptor activity induces in interacting DCs membrane depolarization and calcium influx, which may modulate myeloid cell functions (34, 35). Indeed, calcium mobilization has been shown to increase IL-12 production by DCs upon TLR stimulation (36). Accordingly, coadministration of a calcium ionophore boosted the DC response to IMQ (fig. S7, A and B), analogous to our observations in nociceptor–DC cocultures.

Nociceptors induce transcriptomic changes in DCs

Next, to assess the impact of nociceptors beyond amplifying DC cytokine responses, we performed RNA sequencing (RNAseq) on DCs cultured in the presence or absence of nociceptors, with or without IMQ or capsaicin. A principle component analysis (PCA) revealed that the mere presence of nociceptors induced profound transcriptomic changes in both resting and IMQ-treated cDCs (Fig. 5A). Further marginal changes observable in PCA space were induced by capsaicin stimulation of cocultures, whereas isolated DCs showed altered gene expression profiles only after exposure to IMQ, but not capsaicin. Across all conditions, 983 genes in cDCs were differentially regulated by nociceptors with a fold change (F.C.)≥2 (0.1 FDR). Of the differentially regulated genes, a minority (190 genes) were shared between the IMQ-treated and -untreated groups, indicative of two largely independently regulated genesets: one modulated by nociceptors in immature DCs (445 genes) and a second that only became apparent upon DC activation (348 genes) (Fig. 5, B to D, and fig. S8A). Compared to cocultures with unstimulated nociceptors, capsaicin exposure resulted in only 16 differentially regulated genes in cDCs (F.C.≥2; 0.1 FDR) (fig. S8B), suggesting that nociceptors express most relevant communication molecule(s) constitutively, at least in vitro. Finally, consistent with our earlier observations (fig. S3, A to C), the presence of nociceptors exerted minimal effects on pDCs in which, across all conditions, only 38 genes were differentially expressed (fig. S8, C and D).

Of the differentially regulated genes in IMQ-activated cDCs, the majority were selectively regulated in cDC1s, with a minority shared or unique to cDC2s (Fig. 5C). Gene-set enrichment analysis (GSEA) (37, 38) revealed that among hallmark gene sets (39), the most prominently upregulated pathways in activated cDCs exposed to nociceptors were glycolysis and hypoxia response pathways (fig. S9, A **to** C). This was consistent with the increased proportion of cytokine-producing cells (Fig. 1H and fig. S3C), since these two gene sets correlate with DC activation status (40). Additionally, GSEA revealed a downregulation in the unfolded protein response and apoptotic signaling in activated cDC1s, suggesting that nociceptors may improve activated cDC1 survival. A majority of differentially regulated genes in immature cDCs (Fig. 5D) was likewise regulated in a subset-specific manner. However, the number of genes was comparable between cDC subsets, and a larger number of genes were coregulated. These subset-specific effects of nociceptors likely reflect the fact that cDC1s and cDC2s perform distinct roles in vivo. Of note, the genes coregulated

by nociceptors in cDCs included a number of genes coding for proteins involved in cDC sentinel functions, including pro-IL-1β (fig. S9D and table S1).

CGRP induces an enhanced sentinel phenotype in DCs

Unlike many other pro-inflammatory cytokines, IL-1β is synthesized as a pro-protein (pro-IL-1β) which is proteolytically processed and released upon inflammasome activation (41). Consistent with the lack of overt DC activation in unstimulated cocultures, mature IL-1β was undetectable in coculture supernatants (fig. S10A). However, nociceptors induced a pronounced contact-independent intracellular accumulation of pro-IL-1β in DCs (Fig. 6A), which was reproduced by exposure to nociceptor-conditioned medium (fig. S10B), suggesting the involvement of soluble signal(s) such as neuropeptide(s). Indeed, although SP, PACAP, and VIP were inactive, adrenomedullin and intermedin induced pro-IL-1β expression at submicromolar concentrations and αCGRP was singularly potent even at picomolar concentrations (fig. S10C). Accordingly, CGRP was readily detectable in nociceptor-conditioned medium and further increased after nociceptor stimulation with capsaicin (fig. S10D). Addition of a CGRP receptor antagonist, olcegepant, to nociceptor-conditioned medium attenuated this effect (Fig. 6B). CGRP upregulated pro-IL-1β in DCs within 1 hour, reaching a plateau within 4 hours (fig. S10E). Consequently, CGRP-pretreatment enhanced the release of mature IL-1β from DCs upon inflammasome activation (fig. S10F). Finally, CGRP admixture to IMQ significantly increased pro-IL-1β upregulation in activated DCs as well. Simultaneously, CGRP at high concentrations exerted a moderate inhibitory effect on IL-12 p40 upregulation (fig. S10G). This cytokine pattern implies that the DC response to CGRP is independent of and distinct from canonical DC activation mediated by PAMP receptor ligation.

To further explore the impact of nociceptor-derived CGRP, we compared the transcriptomes of DCs cocultured with nociceptors to those treated with CGRP or SP. Exposure to SP did not significantly alter the transcriptional profile of DCs (Fig. 6C and fig. S11A), in agreement with the present data as well as published datasets (10, 42), which indicate a lack of SP receptors on BMDCs (fig. S11B). Conversely, CGRP treatment resulted in profound transcriptional changes, reminiscent of, but not identical to those observed in nociceptor cocultures (Fig. 6C and fig. S11, A and C), suggesting that CGRP is a major, but not the only nociceptor-derived signal modulating steady-state DCs. The accumulation of CGRP in culture media of unstimulated neuronal cultures (fig. S10D) explains why the transcriptional profile of DC–nociceptor cocultures with or without capsaicin showed only minimal differences (fig. S8B). Owing to the high sensitivity of DCs toward CGRP, the basal CGRP concentration in conditioned medium was apparently sufficient for a full-fledged DC response, rendering a further capsaicin-induced increase in CGRP functionally irrelevant.

CGRP enhances pro-IL-1β in DCs by signaling through a cAMP–p38 dependent pathway.

The CGRP receptor comprises a G protein-coupled receptor (GPCR) as the signal-transducing unit and the receptor-activity modifying protein 1 (RAMP1), which confers ligand specificity (43). Several G-protein subunits interact with this receptor including $\alpha_{i/o}$,

α_q, and α_s. Functionally, $G\alpha_{i/o}$ signaling reduces adenylyl cyclase (AC) activity, whereas $G\alpha_s$ signaling activates AC and promotes cyclic AMP (cAMP) accumulation, activating protein kinase A (PKA) (43) and certain mitogen-activated protein kinases (MAPKs) (44). To determine the pathways involved in CGRP-mediated pro-IL-1β upregulation in DCs, we tested small-molecule inhibitors and activators of the respective enzymes. A PKA inhibitor (H89) showed no effect, whereas a p38 MAPK inhibitor (doramapimod) abrogated CGRP-induced pro-IL-1β expression. Conversely, an AC activator (forskolin) triggered pro-IL-1β expression in DCs, even in the absence of CGRP (Fig. 6D). Both CGRP and forskolin induced rapid phosphorylation of p38 (Fig. 6E), consistent with a model in which p38 activation lies downstream of CGRP-mediated AC activation. Additionally, 8-Br-cAMP, a hydrolysis-resistant synthetic analog of cAMP drove pro-IL-1β accumulation in DCs (fig. S11D) and pertussis toxin-mediated inhibition of $G\alpha_{i/o}$ signaling further potentiated the effect of CGRP (fig. S11E).

Finally, surface-immobilized CCL2 enhanced the DC response to CGRP (Fig. 6E). CCR2 is a $G\alpha_i$-coupled GPCR and, consequently, CCR2 signaling might limit the availability of $G\alpha_i$ subunits, resulting in enhanced $G\alpha_s$ coupling to the CGRP receptor and increased cAMP signaling. Thus, in DCs, CGRP receptor signaling through $G\alpha_s$ promotes cAMP accumulation and initiates a p38-dependent program of gene expression (fig. S11F). Indeed, GSEA confirmed an enrichment of MAPK and p38 MAPK pathway genes in DCs after coculture with nociceptors (fig. S11G). This reprogramming is molecularly distinct from classical activation and renders DCs in a poised state of enhanced sentinel function characterized by intracellular accumulation of pro-IL-1β as well as upregulation of genes important for pathogen resistance, regulation of phagocytosis, cell adhesion and migration, cytokine responsiveness, and antigen presentation (table S1).

Nociceptors promote cytokine production by dermal DCs in vivo.

Having identified three distinct mechanisms—electrical activity, release of CGRP, and secretion of CCL2—by which nociceptors modulate DC functions in vitro, we sought to determine their in vivo relevance by examining mice in which nociceptors had been ablated by treatment with resiniferatoxin (RTX). As shown previously (9) in mice with intact nociceptors, topical treatment with IMQ stimulated the production of IL-12 p40 and an influx of monocytes and neutrophils, a response that was markedly attenuated in RTX-treated animals (Fig. 7A and fig. S12A). Consistent with our in vitro observations, this correlated with a markedly lower frequency of IL-12 $p40^+$ dermal DCs in nociceptor depleted mice (fig. S12B) even though the overall number of dermal DCs in steady-state skin was unaffected (fig. S12C). Similarly, blocking nociceptor electrical activity by topical treatment with lidocaine and QX-314 mimicked the effect of denervation and prevented IMQ induced IL-12 p40 accumulation as well as monocyte and neutrophil influx into the skin (Fig. 7B and fig. S12D). Finally, as predicted in vitro, both nociceptor depletion and anesthetics also decreased the accumulation of IL-6 (Fig. 7, C and D). Thus, the ablation of nociceptors as well as the pharmacological silencing of their electrical activity using topical anesthetics ameliorate the pathology that drives DC-dependent psoriasiform skin inflammation.

CGRP induces pro-IL1β upregulation in dermal DCs in vivo.

In contrast to our in vitro experiments where the presence of nociceptors was sufficient to upregulate pro-IL-1β in DCs (Fig. 6A), the in vivo ablation of nociceptors did not alter baseline levels of pro-IL-1β in dermal DCs (Fig. 7E). This was likely due to the fact that nociceptors in vitro spontaneously release CGRP (45), whereas resting nociceptors in vivo do not (46). Accordingly, when control mice were topically challenged with IMQ, dermal DCs responded by upregulating pro-IL-1β (Fig. 7E), resulting in the accumulation of mature IL-1β in the tissue (Fig. 7F). By contrast, IMQ had only a minimal effect on pro-IL-1β expression and IL-1β accumulation in animals in which nociceptors had been depleted (Fig. 7, E and F) or silenced (Fig. 7, G and H), in a manner analogous to the IL-12 p40 response. However, local treatment with capsaicin, a stimulus for nociceptors, but not DCs, failed to induce IL-12 p40 (fig. S12E), whereas pro-IL-1β was readily upregulated in nociceptor-sufficient animals, an effect that was significantly dampened in RTX-treated mice (Fig. 7I). These findings were in line with our in vitro observations that neuronal activation alone was insufficient to drive IL-12 p40 expression in otherwise unstimulated DCs (Fig. 1I). Capsaicin treatment weakly induced pro-IL-1β upregulation also in RTX-treated animals (Fig. 7I), possibly owing to incomplete nociceptor depletion, or capsaicin-mediated activation of cutaneous mast cells, which may express TRPV1 (47), as well as CGRP (fig. S12F) and other factors that could induce pro-IL-1β upregulation in DCs (48).

To test if the induction of pro-IL-1β in DCs in vivo is CGRP-dependent, we induced sterile tissue inflammation by intradermal corn oil injection. Admixture of olcegepant to the injectate decreased pro-IL-1β upregulation in DCs, but had no impact on the influx of inflammatory cells (Fig. 7J and fig. S12G). Thus, the activation of nociceptors and resultant local release of CGRP are sufficient to drive pro-IL-1β upregulation in dermal DCs independently of other inflammatory signals.

Nociceptor-derived CCL2 controls DC-dependent dermal immune responses

Finally, we assessed the role of nociceptor-derived CCL2. First, to interrogate CCL2 expression in nociceptors, we examined *Ccl2-mCherry*$^{fl/fl}$ reporter mice which express a CCL2-mCherry fusion protein deletable by Cre recombinase (49). CCL2-mCherry was readily detectable by confocal microscopy within intra-axonal vesicle-like structures in cutaneous fibers at steady state (Fig. 8A) and after IMQ treatment (fig. S13A). CCL2 expression was not restricted to nociceptors, indicating that nociceptors are not the sole source of CCL2 in murine skin. Indeed, when *Ccl2-mCherry*$^{fl/fl}$ mice were crossed with *Scn10a*$^{Cre/+}$ mice (hereafter called NaV1.8$^{\Delta CCL2}$), the CCL2 reporter signal in non-neuronal cells remained unchanged, but was extinguished in cutaneous nerve fibers (Fig. 8B and fig. S13B).

Upon topical treatment with IMQ, NaV1.8$^{\Delta CCL2}$ animals exhibited smaller inflammatory infiltrates (Fig. 8C) and decreased IL-12 p40 acumulation in the skin (Fig. 8D) compared to Cre-negative littermates. Dermal DCs expressed high levels of CCR2 (fig. S13C), indicating

that they were equipped to sense and respond to CCL2. Nonetheless, the number of DCs in unperturbed skin was comparable between NaV1.8$^{\Delta CCL2}$ animals and littermate controls (fig. S13D), suggesting that nociceptor-derived CCL2 was dispensable for the maintenance of dermal DCs under steady-state conditions. After IMQ treatment, however, NaV1.8$^{\Delta CCL2}$ mice showed a decrease in dermal DC numbers as compared to littermates (Fig. 8E), suggesting that nociceptor-derived CCL2 serves as a retention signal preventing DCs from prematurity leaving the skin, allowing for a longer period of in situ cytokine production and more pronounced local inflammation.

In addition to compromising local inflammatory responses, we reasoned that the dysregulation of DC migration may also interfere with the acquisition of cutaneous antigens and affect the initiation of adaptive immune responses. To test this idea, we performed contact hypersensitivity (CHS) experiments where the adaptive recall response depends on the acquisition of hapten-modified self-antigens by dermal DCs and their presentation to adaptive lymphocytes in draining lymph nodes (50). In naïve mice, hapten exposure of ear skin caused a comparable irritant response in NaV1.8$^{\Delta CCL2}$ animals and littermates. By contrast, the DC-dependent recall response in mice sensitized by prior hapten painting of abdominal skin was nearly abrogated in the absence of nociceptor-derived CCL2 (Fig. 8F and fig. S13E). Nociceptor ablation has previously been shown to impair the ability of DCs to acquire viral antigens in HSV-1 infected skin (51), suggesting that this phenotype of NaV1.8$^{\Delta CCL2}$ mice was likely due to a defect in DC-dependent priming of antigen-specific lymphocytes in lymph nodes. Indeed, when WT mice were treated with lidocaine and QX-314 to transiently inhibit nociceptor activity in abdominal skin during sensitization, we observed that the CHS response was compromised in subsequently challenged ear skin where nociceptors had always been fully functional (Fig. 8G and fig. S13F). Thus, nociceptors must be functional and express CCL2 for the proper induction of both DC-dependent local inflammation and the priming of adaptive immune responses against dermal antigens.

Discussion

At the transcriptome level, our results indicate that the presence of nociceptors induces numerous subset-specific changes in cDC1 and cDC2 cells in vitro. These differential responses likely reflect the fact that cDC1s and cDC2s have distinct roles in regulating immune responses and it will be important to determine whether and how nociceptors regulate subset-specific cDC functions in vivo. The present study has, however, focused on exploring the communication signals emanating from nociceptors that elicit a shared response by all cDCs in peripheral tissues.

We show that nociceptors control DC functions in a context-dependent manner through at least three independent communication modalities. Without immune stimuli, nociceptor-derived CGRP induces transcriptional changes in steady-state DCs to upregulate sentinel function-related genes but without causing overt DC activation. Upon concomitant encounter of painful stimuli and PAMPs, the nociceptors' electrical activity is sensed by interacting PAMP-stimulated DCs, which increases the proportion of DCs that commence production of pro-inflammatory cytokines. Thus, DCs are uniquely equipped to sense and interpret

nociceptor activation either as a "reminder" to assume a poised, anticipatory state when other inflammatory signals are absent or as an “alarm call” that amplifies their collective inflammatory response to immune stimuli. Additionally, by secreting CCL2, nociceptors further fine-tune DC functions by promoting their contribution to local inflammatory responses and by regulating the egress of DCs from the skin to optimize adaptive immune responses (fig. S14).

CGRP receptor-mediated activation of AC (52) exerts anti-inflammatory effects on immune cells including macrophages (53), neutrophils (46), γδT cells (54), and innate lymphoid cells (ILCs) (55). By contrast, we observed that CGRP, even at high concentrations, had only modest inhibitory effects on IL-12 p40 upregulation in activated BMDCs (figs. S4E and S10G). This was in contrast to previously reported inhibitory effects of CGRP on IL-12 production in GM-CSF-induced BMDCs (11). Unlike the Flt3L-induced BMDCs used here, GM-CSF cultures contain macrophages (56), which, are potently inhibited by nociceptors (Fig. 1D) as well as by CGRP (52). It is therefore possible that the negative effect of CGRP on GM-CSF-induced BMDC cultures may be a consequence of macrophage contamination rather than a true effect on DCs. Finally, taken at face value, these observations also suggest an inherent difference in the intracellular signaling pathways between DCs and macrophages, whereby AC activation may exert strong inhibitory effects on the latter (57) but not the former.

In light of the exquisite sensitivity of DCs toward CGRP, the close proximity of DCs and nociceptors in vivo, and the anticipatory nature of the DC response elicited by CGRP, it is tempting to speculate that DCs may have specifically evolved to register and interpret a local, limited release of CGRP induced by transient or subtle activation of nociceptors as a warning signal that could portend a barrier breach. By contrast, other immune cells that do not a priori associate closely with nociceptors may only sense CGRP when it is released in larger quantities, likely as a consequence of severe tissue damage. In this context, CGRP-induced anti-inflammatory and tissue repair-promoting functions (e.g., via action on macrophages (57) or neutrophils (46)) may become more prominent.

Although CGRP did not induce IL-23 production by DCs in this study, recent work has demonstrated that nociceptor-derived CGRP is sufficient and necessary for IL-23 production by CD301b$^+$ dermal DCs during *C. albicans* infecion (8). The reasons for this discrepancy remain unclear, but it is possible that CGRP-induced IL-1β potentiates IL-23 expression (58, 59) or that intermediary cell type(s) may be involved, which generate as-yet-unidentified secondary signals in response to CGRP to promote IL-23 production by DCs.

Aside from neuropeptides, our results highlight a critical role for CCL2, a chemokine whose expression by nociceptors has traditionally been considered a sign of pathology. CCL2 can recruit inflammatory cells to DRGs, resulting in peripheral sensitization and neuropathic pain (60). However, some nociceptors express CCL2 even at steady state, at least at the mRNA level (3, 61, 62). Indeed, we show here that the expression of CCL2 in cutaneous fibers is not necessarily maladaptive but rather serves to fine-tune DC-dependent immune responses. Aside from DCs, other cell types including monocytes and memory T-cell subsets also express the CCL2 receptor, CCR2, however, the impact of nociceptor derived CCL2

on these populations remains to be explored. Moreover, further work will be needed to determine how CCL2 is regulated in nociceptors. In vitro, cultured nociceptors released CCL2 spontaneously and nociceptor stimulation further potentiated CCL2 release, similar to the dynamics of neuropeptide release. In vivo, neuropeptide release from nociceptors is tightly controled (46), but it remains to be established whether similar rules apply also to CCL2.

Although myeloid leukocytes are generally not considered excitable, we observed that activation of nociceptors induced membrane depolarization and calcium flux in the interacting DCs. Spreading of action potentials to and among non-neural cells through mechanisms including gap junctions and tunneling nanotubes has been described previously (63) and both of these communication modalities have been reported for DCs (64). Whatever the mechanism, our observations establish a precedent for a direct, contact-dependent, and neuropeptide-independent communication pathway between nociceptors and DCs, which culminates in calcium mobilization in the latter. Intracellular calcium is a key second messenger in numerous signaling processes. The downstream molecular signaling pathway(s) promoting DC production of IL-12 p40 and IL-6 but not TNFα remain(s) to be clarified. Nonetheless, synergy between MyD88 and TRIF-dependent pathways in DCs has previously been shown to stimulate IL-12 and IL-6 secretion, while having no effect on TNFα (65), indicating that these cytokines are not coregulated. Conceivably, calcium mobilization in activated DCs triggered by firing nociceptors might act in an analogous manner to synergize with TLR induced MyD88 signaling to potentiates the expression of IL-12 p40 and IL-6.

Materials and Methods

Mice

C57BL/6J (JAX stock #000664), *Ccl2*$^{-/-}$ (JAX stock #004434) (26), *Tlr7*$^{-/-}$ (JAX stock #008380) (17), *Zbtb46*^{eGFP} (JAX stock #027618) (30), and *Ccl2-mCherry*$^{fl/fl}$ (JAX stock #016849) (69) mice were purchased from Jackson Laboratory. *I–A*^{b}β-eGFP (66), *Scn10a*^{Cre} (67) and *Scn10a*$^{Cre/Cre}$*Rosa26*$^{TdT/TdT}$ (3) mice were all described previously and were bred at the Harvard Medical School animal facility. All animal experiments were performed in accordance with national and institutional guidelines, and were approved by the IACUC and COMS of the Harvard Medical School. Both male and female mice were used.

In vitro DC generation

Flt3L-induced bone marrow-derived dendritic cells were generated as described previously (68). Briefly, bone marrow was harvested from femurs and tibiae of 6-to-8-week-old C57BL/6J mice of either sex. Red blood cells were lysed and bone marrow cells were plated with 100 ng/ml of recombinant Flt3L (R&D Systems) in six-well plates (3 ml per well), one plate per mouse in RPMI1640 medium (Gibco) containing 10% FBS (Gemini Bio), β-mercaptoethanol, glutamine and penicillin–streptomycin. Fully developed DCs were harvested and used on days 9-10.

In vitro macrophage generation

MCSF-induced bone marrow macrophages were generated as described previously (69). Briefly, bone marrow was harvested from femurs and tibiae of 6-to-8-week-old C57BL/6J mice of either sex. Red blood cells were lysed and bone marrow cells were plated with 25 ng/ml of recombinant M-CSF in six-well plates (3 ml per well) in RPMI1640 medium (Gibco) containing 10% FBS (Gemini Bio), β-mercaptoethanol, glutamine, and penicillin–streptomycin. Fully developed macrophages were harvested and used on day 7.

In vitro nociceptor culture

DRG cultures were prepared from freshly isolated dorsal root ganglia from adult (6-to-10-week-old) C57BL/6J mice of either sex as described previously (45, 70) with minor modifications. Briefly, the dissection was performed in ice-cold PBS and harvested DRGs were kept on ice throughout. The first step of digestion was performed for 10 min at 37°C in 3 ml of HBSS (Gibco) with 60 U of papain (Worthington), 0.5 mM EDTA, and 1.5 mM $CaCl_2$. The second digestion step was performed in 3 ml of HBSS with 4 mg/ml of collagenase Type-2 (Worthington) and 5 mg/ml of dispase (Gibco) for 30 min at 37°C. Cell suspensions were triturated by repeated pipetting in Leibovitz medium (Gibco) supplemented with 10% FBS (Gemini Bio), overlaid over 20% Percoll (GE Healthcare) in Leibovitz medium, and centrifuged for 9 min at 400*g* with no brake. Pelleted cells were washed in neurobasal medium (Gibco) containing B27 supplement (Gibco) and penicillin–streptomycin before being plated (1-1.5×10^4 cells per well) in wells precoated with poly-D lysine and laminin (both Sigma Aldrich) in neurobasal medium containing B27 supplement and penicillin–streptomycin, supplemented with 5 μM cytosine β-D-arabinofuranoside (Sigma-Aldrich) and 25 ng/ml of mouse recombinant NGF (R&D Systems). Culture medium was refreshed every 4-5 days and neuronal culture was typically used between days 7 and 10 post-plating. Cultures were visually inspected to verify neuronal recovery as well as depletion of contaminating glial/Schwann cells prior to each experiment.

In vitro cortical and hippocampal neuron cultures

CNS neuronal cultures were prepared from freshly isolated C57BL/6J mouse embryonal (E18-19) brains as described previously (71) with minor adjustments. Dissection was performed in ice-cold HBSS + HEPES (both Gibco) and tissues were digested at 37°C for 15 min in 0.25% trypsin (Invitrogen) for hippocampus and 0.25% trypsin + 0.5 mg/ml DNAse I (Roche) for cortex samples. Tissues were homogenized by trituration in a fire-polished Pasteur pipette and single-cell suspensions were generated by filtration through 100-μm cell strainers. Cells were washed in neurobasal medium containing B27 supplement (both Gibco) and penicillin–streptomycin before being plated in wells precoated with poly-D lysine and laminin (both Sigma-Aldrich) in neurobasal medium containing B27 supplement and penicillin–streptomycin supplemented with 5 μM cytosine β-D-arabinofuranoside (Sigma-Aldrich). Culture medium was refreshed every 3 days and the culture was used between days 7 and 14 post-plating.

In vitro cocultures

For coculture experiments, neuronal medium was replaced with fresh neurobasal medium containing B27 supplement and penicillin–streptomycin and 1×10^5 BMDCs per well were added in an equal volume of RPMI1640 medium containing 10% FBS, β-mercaptoethanol, glutamine and penicillin–streptomycin. Cells were allowed to interact for 2-4 hours before any treatments/stimuli were applied, unless stated otherwise. As a control, DCs were plated and treated in an identical fashion in wells containing appropriate volume of neurobasal medium containing B27 supplement and penicillin–streptomycin but no nociceptors.

In vitro treatments

All treatments were performed overnight unless otherwise stated. All CGRP treatments were performed with 1 nM CGRP unless otherwise indicated. Lidocaine (500 μM), QX314 (1 mM), A967079 (10 μM), and olcegepant (100 nM) were added to cultured nociceptors 2 hours prior to the addition of DCs. H89 (1 μM), doramapimod (1 μM), and pertussis toxin (100 ng/ml) were added to DCs immediately prior to CGRP treatment. 8-Br-cAMP (1 mM) and forskolin (50 μM) were used without further stimuli. A23187 (400 ng/ml) was added to DCs alongside IMQ and the treatment lasted for 4 to 5 hours to avoid toxicity. Activating stimuli were used at following concentrations: IMQ (1 μg/ml), zymosan (10 μg/ml), LPS (1 ng/ml), flagellin (20 ng/ml), CpG (0.1 μM), poly I:C (1 μg/ml), PR-8 GFP IAV (multiplicity of infection (M.O.I.) 0.25), *S. pneumoniae* (M.O.I. 5), and *C. albicans* (M.O.I. 10).

Microbes

Influenza PR8-GFP was generously provided by Dr. A. Garcia-Sastre at the Mount Sinai School of Medicine and the NIAID Centers of Excellence for Influenza Research and Surveillance program. *S. pneumoniae* was a kind gift from Dr. R. Malley at the Boston Children's Hospital and Harvard Medical School. *C. albicans* was purchased from ATCC (MYA-2876).

ELISA

Elisa kits specific for IL-12 p40 (Cat #431601), IL-6 (Cat #431302), TNFα (Cat # 430902), IFNβ (Cat # 439407), CCL2 (Cat #432704), and IL-1β (Cat #432603) were from Biolegend. The EIA kit specific for CGRP (Cat #589001) was from Cayman Chemicals. All assays were performed as per manufacturers' instructions.

In vitro coculture flow cytometry analysis

In vitro cultures were harvested in warm 5 mM EDTA in PBS. Dead cells were then stained using the LIVE/DEAD Fixable Near-IR Dead Cell Stain Kit (Thermo Fisher) in ice-cold PBS. Samples were washed and stained with fluorescent antibodies for appropriate surface markers in FACS buffer (1% FCS, 5 mM EDTA, and 0.1% NaN_3 in PBS) on ice. Intracellular staining was performed using the Cytofix/Cytoperm kit (BD Biosciences) according to the manufacturer's instructions. cDC1s were identified as XCR-1^+ and cDC2s were identified as $CD11b^+$. For IL-6 intracellular stains, 10 μM Brefeldin A was added to the cultures 2 hours prior to harvest.

Transwell assays

BMDCs ($0.5\text{-}1\times10^6$) in complete RPMI1640 medium were added to the upper compartment of a transwell setup (Corning) with 5 μm pores and allowed to migrate into the lower compartment containing chemotactic stimuli for 4 hours. Migrated cells were harvested, stained with fluorescent antibodies and enumerated by flow cytometry. The chemotactic index was calculated as the number of cells transmigrated under a given condition divided by the number of cells that transmigrated between two compartments containing the same medium.

Chemotactic molecule identification

Mouse Chemokine Array C1 (Ray Biotech) and Proteome Profiler Mouse Chemokine Array Kit (R&D) were used. Membranes were incubated with nociceptor-conditioned medium or control medium overnight and developed as per manufacturers' instructions. The signal intensity for each spot was quantified in Fiji 2.0.0 (72) using the Analyze Gels function.

SDS-PAGE and immunoblot analysis

Cells were harvested and lysed for 30 min in Tris buffer pH7.5 with 1% SDS, 150 mM NaCl, 10 mM NaF, 2 mM Na_3VO_4, protease inhibitors (Thermo Scientific), and benzonase (Sigma Aldrich). After 30 min, the lysate was diluted 1 to 10 into Tris buffer pH 7.5 with 1% NP40, 150 mM NaCl, 10 mM NaF, 2 mM Na_3VO_4, and protease inhibitors (Thermo Scientific) and centrifuged for 15 min at 16,000*g*. Supernatants were prepared for SDS-PAGE in 6X Laemmli buffer (60% (v/v) glycerol, 150 mg/ml SDS, 0.75 mg/ml bromophenol blue in 75 mM Tris–HCl pH 6.8) in the presence of 100 mM DTT. Separation was carried out using 4 to 12% NuPAGE precast gels (Invitrogen). Proteins were transferred onto Immobilon P membrane (Merck Millipore) using wet transfer and the membrane was blocked in 5% BSA in PBS + 0.05% Tween-20. Binding of appropriate HRP-conjugated antibodies was revealed using Luminata Forte HRP substrate (Merck Millipore) and Amersham Imager 600 (GE Healthcare).

Live-cell imaging

Live-cell imaging was performed on a Nikon Ti inverted microscope equipped with W1 Yokogawa Spinning disk with 50-μm pinholes, Andor Zyla 4.2 Plus sCMOS monochrome camera and OKO Lab Heated enclosure with environmental control set to 37°C and 5% CO_2. Plan Apo λ 20X/0.75 DIC I objective was used. All imaging experiments were performed in a 1:1 mixture of RPMI1640 medium containing 10% FBS, β-mercaptoethanol, glutamine and penicillin–streptomycin and neurobasal medium containing B27 supplement and penicillin–streptomycin, both phenol red-free, on μ-Slide eight-well chambered coverslips (Ibidi). For the microfluidics experiments, Xona Microfluidics chips with 150-μm microgrooves were used.

For calcium imaging experiments, cells were loaded with 10 μM Fluo-4 calcium-sensitive dye (Thermo-Fisher) for 20 min at 37°C. Immediately before imaging, Fluo-4 containing medium was replaced with fresh, prewarmed, phenol red-free medium and Fluo-4 signal was imaged in a single confocal plane using 488-nm laser line and GFP filter cube (Chroma ET 49002).

For membrane potential imaging experiments using BeRST dye, cells were loaded with 5 μM BeRST and 10 μM Fluo-4 for 20 min at 37°C. Immediately before imaging, dye-containing medium was replaced with fresh, prewarmed phenol red-free medium and images were acquired in a single confocal plane using 488-nm and 640-nm laser lines and GFP and Cy5 filter cubes (ET Chroma 49002 and 49006).

For membrane potential imaging experiments using Di-8-ANNEPS, cells were loaded with 5 μM Di-8-ANNEPS for 30 min at 37°C. Immediately before imaging, dye-containing medium was replaced with fresh, prewarmed medium and images were acquired in a single confocal plane using 488-nm laser line and mCherry and Cy5 filter cubes (ET Chroma 49008 and 49006).

Light-sheet imaging

The lattice light-sheet microscope was constructed as described previously (73) with a Special Optics, 0.65 NA, excitation objective and a Nikon, CFI Apo LWD 25XW, 1.1 NA detection objective, an Orca Flash 4.0 v3 sCMOS camera (Hamamatsu), and 488-nm (300 mW Coherent Sapphire) and 560-nm (500 mW, MPB Communications) lasers. The annular mask was set at 0.42-0.5 NA and a square lattice in the dithered mode was produced at the sample. The excitation power (488 nm) was measured at the back focal plane of the excitation objective at ~100 μW. The 25X detection objective was paired with a 500-mm achromat lens for an effective magnification of 63.7X, resulting an image pixel size of 102 nm. The exposure time for each plane was 4 ms and the stage-scanning step size for the volumetric imaging was 0.5 mm, corresponding to 265 nm along the optical axis after deskewing. Data was deskewed and deconvolved with LLSpy (DOI: 10.5281/zenodo.1059099) and cudaDeconv (source code available at https://github.com/scopetools/cudaDecon) using a PSF measured from a 0.1μm bead. sCMOS residual charge artifact was corrected using LLSpy (https://llspy.readthedocs.io/en/latest/camera.html).

Electron microscopy

Nociceptors were grown on aclar coverslips precoated with poly-D lysine and laminin. DCs were allowed to interact with nociceptors for 4 hours before the coculture was fixed in a mixture of 2.5% glutaraldehyde, 1.25% paraformaldehyde, and 0.03% picric acid in 0.1 M sodium cacodylate buffer (pH 7.4) for 1 hour at RT. The cells were washed in 0.1 M sodium cacodylate buffer (pH 7.4), postfixed for 30 min in a 1% OsO_4– 1.5% $KFeCN_6$ solution, washed twice in water and once in maleate buffer, and incubated in 1% uranyl acetate in maleate buffer for 30 min. This was followed by two washes in water and subsequent dehydration in grades of alcohol (5 min each: 50%, 70%, 95%, and twice 100%). The samples were subsequently embedded in TAAB Epon (Marivac Canada Inc.) and polymerized at 60°C for 48 hours. After polymerization, the aclar was peeled off and ultrathin sections (approximately 80 nm) were cut on a Reichert Ultracut-S microtome, picked up on to copper grids and stained with lead citrate. Grids were examined under a $TecnaiG^2$ Spirit BioTWIN transmission electron microscope and images were recorded using an AMT 2k CCD camera.

Confocal imagining

For whole-mount imagining of dermal sheets, ears of from $Zbtb46^{eGFP}Scn10a^{Cre/+}ROSA^{tdTomato/+}$ animals were split into the dorsal and ventral aspects, fixed in 4% PFA, permeabilized in 0.3% Tween in PBS, and stained with S100β primary antibody overnight in a blocking buffer containing 3% BSA. Samples were washed and stained with anti-rabbit Alexa Fluor 647 and anti-GFP Alexa Fluor 488 antibodies. Ears of $CCL2\text{-}RFP^{flox}$ or $Scn10a^{Cre/+}CCL2\text{-}RFP^{flox}$ animals were split into the dorsal and ventral aspects, fixed in 4% PFA, permeabilized in 0.3% Tween in PBS, blocked in 3% BSA, and stained with β3-Tubulin and mCherry antibodies for 48 hours. Subsequently, the samples were washed and stained with anti-goat Alexa Fluor 568 and anti-rabbit Alexa Fluor 647 antibodies.

For imagining of fixed nociceptor cultures, nociceptors isolated from $NaV1.8^{Cre/+}Rosa26^{tdTomato/+}$ were plated in μ-Slide eight-well chambered coverslip (Ibidi) and cultures were maintained as per the standard protocol. Cells were fixed in 4% PFA, permeabilized in 0.3% Tween in PBS, and stained with β3-tubulin primary antibody overnight in a blocking buffer containing 3% BSA. Samples were washed and stained with an anti-rabbit Alexa Fluor 488 antibody.

Images were acquired on an Olympus IX83 inverted single point laser scanning confocal microscope with UPlan S Apo 20X/0.75 air or UPlan X Apo 60X/1.42 oil objectives.

Image analysis

Calcium imaging as well as membrane potential analysis was performed in Fiji2.0.0 (72). Images are presented using the “Fire” LUT and quantitation of signal was performed in selected ROIs across all time-points using the “Plot Z-axis profile” function to generate single cell response graphs. For statistical analysis, cells were manually traced and were considered “responders” if their Fluo-4 signal showed at least 50% increase ($F_{max}/F_0 \geq 1.5$), “equivocal” for 30 to 50% increase ($1.5 > F_{max}/F_0 \geq 1.3$) and “non-responders” if no change over 30% was observed ($F_{max}/F_0 < 1.3$). Only cells observed contacting a firing axon were considered in the coculture condition.

For the ratiometric analysis of Di-8-ANNEPS imaging, both channels were background-subtracted and ratio of channels was generated for each pixel. The resulting image was thresholded and is presented using the “Fire” LUT. A binary mask created from original images that included all neuronal bodies as well as axons and DCs was used to assign zero value to background pixels. 3D reconstruction of confocal images of skin whole mounts and the generation of surfaces was performed in Imaris 9.2.1.

RNA sequencing

CD45.1 BMDCs were incubated with nociceptors from CD45.2 mice or alone and treated with appropriate stimuli. After 8 hours, the cultured cells were harvested, stained, and sorted on a MoFlo Astrios EQ FACS-sorter (Beckman). cDC1s were identified as $CD45.1^+XCR\text{-}1^+CD11b^-$, cDC2s as $CD45.1^+CD11b^+XCR\text{-}1^-$, and pDCs as $CD45.1^+XCR\text{-}1^-CD11b^-PDCA1^+$. One thousand cells of each population were sorted

directly into 5 μl of lysis buffer (TCL Buffer (Qiagen) with 1% β-mercaptoethanol) and Smart-seq2 libraries were prepared as previously described (74, 75) with slight modifications. Briefly, total RNA was captured and purified on RNAClean XP beads (Beckman Coulter). Polyadenylated mRNA was then selected using an anchored oligo(dT) primer (5′-AAGCAGTGGTATCAACGCAGAGTACT30VN-3′) and converted to cDNA via reverse transcription. First strand cDNA was subjected to limited PCR amplification followed by transposon based fragmentation using the Nextera XT DNA Library Preparation Kit (Illumina). Samples were PCR amplified for 18 cycles using barcoded primers such that each sample carried a specific combination of eight base Illumina P5 and P7 barcodes and pooled together prior to sequencing. Paired-end sequencing was performed on an Illumina NextSeq500 using 2×25 bp reads.

RNAseq data analysis

Reads were aligned to the mouse genome (GENCODE GRCm38/mm10 primary assembly and gene annotations vM16; https://www.gencodegenes.org/mouse_releases/16.html) with STAR 2.5.4a (https://github.com/alexdobin/STAR/releases). The ribosomal RNA gene annotations were removed from GTF (General Transfer Format) file. The gene-level quantification was calculated by featureCounts (http://subread.sourceforge.net/). Raw reads count tables were normalized in iDEP.91 (EdgeR (Log2(CPM+1))) (76). Samples with less than 2×10^6 uniquely mapped reads were excluded to mitigate the effect of poor quality samples on normalized counts, and only genes with minimal 50 counts per million (CPM) expression in at least two libraries were selected for further analysis to exclude genes with little to no expression across all conditions. Differentially expressed genes were identified using DESeq2 with F.C.≥2 and FDR 0.1 cutoffs in iDEP.91. Principle component analysis was performed and visualized using Population PCA software (http://cbdm.hms.harvard.edu/LabMembersPges/SD.html) for 3D PCA, or prcomp function within the R3.6.1 package and visualized using ggbiplot for 2D PCA. Morpheus (https://software.broadinstitute.org/morpheus/) was used for visualization and heatmap generation. GSEA analysis (37, 38) was performed in GSEA 4.0.1 software using the Hallmarks gene matrix v7.1 (h.all.v7.1) (39) and the Biocarta gene matrix v7.4 (c2.cp.biocarta.v7.4) MAPK_PATHWAY and P38 MAPK PATHWAY subsets.

Antibodies

All antibodies used in this study are listed in table S2.

In vivo nociceptor depletion

RTX-mediated depletion of nociceptor innervation was performed as published previously (9). Four-week-old mice were injected on 3 consecutive days with 30, 70, and 100 mg per kilogram of body weight of RTX or vehicle control and allowed to age for at least 6 weeks before being used for experiments. Functional denervation was confirmed using the tail withdrawal assay (9).

Imiquimod and capsaicin treatment in vivo

Eight-to-twenty-week-old C57BL/6J mice were treated topically with capsaicin or IMQ as published previously (9, 77). Briefly, for capsaicin treatment, mice were anaesthetized and 250 μg of capsaicin (50 mM in DMSO) was applied to the treated ear (125 μg on each side) twice, 12 hours apart. Pro-IL-1β expression was assessed 24 hours after the first dose. For IMQ treatment, mice were anaesthetized and 25 mg of IMQ in the form of a 5% cream (Aldara) was applied to the treated ear three times, 24 hours apart. Where indicated, 3 hours before the IMQ treatment, 5 mg of QX-314 and 5 mg of lidocaine in the form of 4% cream (Aspercreme) was applied to the treated skin. IL-1β, pro-IL-1β, IL-6, or IL-12 p40 expression was assessed 72 hours after the first treatment.

Intradermal injections

Six-to-ten-week-old C57BL/6J mice were anesthetized and 10 μl of PBS, corn oil with 10% DMSO, or corn oil with 10% DMSO and 5 mg/ml of olcegepant was injected intradermally into the dorsal side of the ear pinna. After 16 hours, the animals were sacrificed and the injected area of the ear was separated and prepared for flow cytometry analysis.

Skin flow cytometry analysis

Mouse ears were split into the dorsal and ventral aspects, cut into small pieces and incubated for 40-60 min at 37°C and constant shaking in RPMI 1640 medium containing DNase (100 μg/ml) and TM Liberase (62.5 μg/ml) or DNase (100 μg/ml) and collagenase D (2.5 mg/ml). Single-cell suspensions were generated using GentleMACS dissociator (Miltenyi) and mechanical disruption was then performed using 50-μm cell strainers. Single-cell suspensions were kept on ice, dead cells were identified using the LIVE/DEAD Fixable Near-IR Dead Cell Stain Kit (Thermo Fisher), Fc receptors were blocked with the anti-CD16/32 antibody, and surface markers were stained with appropriate fluorescent antibodies in FACS buffer (1% FCS, 5 mM EDTA, and 0.1% NaN_3). Intracellular staining was performed using the Cytofix/Cytoperm kit (BD Biosciences) as per manufacturer's instructions. DCs were identified as $CD45^+CD11c^+MHC\text{-}II^+CD64^-Ly6C^-$, monocytes as $CD45^+CD3^-CD19^-NK1.1^-Ly6C^{hi}Ly6G^-$, and neutrophils as $CD45^+CD3^-CD19^-NK1.1^-Ly6C^{lo}Ly6G^+$.

Contact hypersensitivity

CHS experiments were performed as described previously (78). Briefly, abdomens of 8-to-12-week-old C57BL/6J mice were shaved and sensitized the following day with 50 μl of 0.5% 2,4-dinitro-1-fluorobenzene (DNFB) in acetone or vehicle control. For experiments with lidocaine + QX314, 5 mg of QX314 and 5 mg of lidocaine in the form of 4% cream (Aspercreme) were applied to the shaved skin 4 hours prior to sensitization and in 24-hour intervals thereafter for the following 2 days. On day 5, mouse ears were challenged with 20 μl of 0.2% DNFB in acetone or vehicle control, and ear thickness was measured for the following 4-5 days. Antigen specific ear swelling was calculated as: [DNFB-treated ear thickness – control ear thickness]. The experimenter performing ear swelling measurements was blinded as to the genotype of mice and treatement group.

Statistical analysis

Statistical analyses were performed as indicated in figure legends. Student's *t* test was used for statistical comparisons of two experimental groups. If more than two experimental groups were present, one-way analysis of variance (ANOVA) with Tukey's multiple comparisons test was used. For analyses that included two independent variables, two-way ANOVA with Tukey's multiple comparisons test was used. All statistical analyses were performed in GraphPad Prism 9.3.1.

Supplementary Material

Refer to Web version on PubMed Central for supplementary material.

Acknowledgments:

We thank Dr. H. Ploegh for sharing MHC-II eGFP mice, members of the von Andrian lab for helpful advice and discussions and Harvard Medical School Electron Microscopy, Flow Cytometry, Microscopy Resources on the Northern Quad (MicRoN) and Cell Biology Microscopy facilities for technical assistance. Influenza PR8-GFP was generously provided by Dr. A. Garcia-Sastre at the Mount Sinai School of Medicine and the NIAID Centers of Excellence for Influenza Research and Surveillance program. *Streptococcus pneumoniae* was a kind gift from Dr. R. Malley at the Boston Children's Hospital and Harvard Medical School.

Funding:

National Institutes of Health grant AR068383 (U.H.v.A.), National Institutes of Health grant R01NS098088 (E.W.M.), CRI Irvington postdoctoral fellowship CRI2453 (P.H.), Howard Hughes Medical Institute Gilliam Fellowship (G.O.)

Data and materials availability:

RNA-seq data are available in the Gene Expression Omnibus (GEO) under GSE 217503, subseries GSE 217500 (data shown in Fig. 5) and GSE 217502 (data shown in Fig. 6C). All data are available in the main text or the supplementary materials.

References:

1. Baral P, Udit S, Chiu IM, Pain and immunity: implications for host defence. Nat Rev Immunol 19, 433–447 (2019). [PubMed: 30874629]
2. Ordovas-Montanes J et al. , The Regulation of Immunological Processes by Peripheral Neurons in Homeostasis and Disease. Trends Immunol 36, 578–604 (2015). [PubMed: 26431937]
3. Huang S et al. , Lymph nodes are innervated by a unique population of sensory neurons with immunomodulatory potential. Cell 184, 441–459 e425 (2021). [PubMed: 33333021]
4. Pinho-Ribeiro FA, Verri WA Jr., Chiu IM, Nociceptor Sensory Neuron-Immune Interactions in Pain and Inflammation. Trends Immunol 38, 5–19 (2017). [PubMed: 27793571]
5. Woolf CJ, Ma Q, Nociceptors--noxious stimulus detectors. Neuron 55, 353–364 (2007). [PubMed: 17678850]
6. Veiga-Fernandes H, Mucida D, Neuro-Immune Interactions at Barrier Surfaces. Cell 165, 801–811 (2016). [PubMed: 27153494]
7. Cabeza-Cabrerizo M, Cardoso A, Minutti CM, Pereira da Costa M, Reis e Sousa C, Dendritic Cells Revisited. Annu Rev Immunol 39, 131–166 (2021). [PubMed: 33481643]
8. Kashem SW et al. , Nociceptive Sensory Fibers Drive Interleukin-23 Production from CD301b+ Dermal Dendritic Cells and Drive Protective Cutaneous Immunity. Immunity 43, 515–526 (2015). [PubMed: 26377898]

9. Riol-Blanco L et al. , Nociceptive sensory neurons drive interleukin-23-mediated psoriasiform skin inflammation. Nature 510, 157–161 (2014). [PubMed: 24759321]
10. Perner C et al. , Substance P Release by Sensory Neurons Triggers Dendritic Cell Migration and Initiates the Type-2 Immune Response to Allergens. Immunity 53, 1063–1077 e1067 (2020). [PubMed: 33098765]
11. Tsujikawa K et al. , Hypertension and dysregulated proinflammatory cytokine production in receptor activity-modifying protein 1-deficient mice. Proc Natl Acad Sci U S A 104, 16702–16707 (2007). [PubMed: 17923674]
12. Zelenay S, Reis e Sousa C, Adaptive immunity after cell death. Trends Immunol 34, 329–335 (2013). [PubMed: 23608152]
13. Binshtok AM et al. , Coapplication of lidocaine and the permanently charged sodium channel blocker QX-314 produces a long-lasting nociceptive blockade in rodents. Anesthesiology 111, 127–137 (2009). [PubMed: 19512868]
14. Gibson SJ et al. , Plasmacytoid dendritic cells produce cytokines and mature in response to the TLR7 agonists, imiquimod and resiquimod. Cell Immunol 218, 74–86 (2002). [PubMed: 12470615]
15. Hemmi H et al. , Small anti-viral compounds activate immune cells via the TLR7 MyD88-dependent signaling pathway. Nat Immunol 3, 196–200 (2002). [PubMed: 11812998]
16. Liu T, Xu ZZ, Park CK, Berta T, Ji RR, Toll-like receptor 7 mediates pruritus. Nat Neurosci 13, 1460–1462 (2010). [PubMed: 21037581]
17. Lund JM et al. , Recognition of single-stranded RNA viruses by Toll-like receptor 7. Proc Natl Acad Sci U S A 101, 5598–5603 (2004). [PubMed: 15034168]
18. Esancy K et al. , A zebrafish and mouse model for selective pruritus via direct activation of TRPA1. Elife 7, (2018).
19. Wei JJ et al. , Activation of TRPA1 nociceptor promotes systemic adult mammalian skin regeneration. Sci Immunol 5, (2020).
20. Deng L, Chiu IM, Microbes and pain. PLoS Pathog 17, e1009398 (2021). [PubMed: 33793668]
21. Maruyama K et al. , The ATP Transporter VNUT Mediates Induction of Dectin-1-Triggered Candida Nociception. iScience 6, 306–318 (2018). [PubMed: 30240621]
22. Meseguer V et al. , TRPA1 channels mediate acute neurogenic inflammation and pain produced by bacterial endotoxins. Nat Commun 5, 3125 (2014). [PubMed: 24445575]
23. Assas BM, Pennock JI, Miyan JA, Calcitonin gene-related peptide is a key neurotransmitter in the neuro-immune axis. Front Neurosci 8, 23 (2014). [PubMed: 24592205]
24. Suvas S, Role of Substance P Neuropeptide in Inflammation, Wound Healing, and Tissue Homeostasis. J Immunol 199, 1543–1552 (2017). [PubMed: 28827386]
25. Ganea D, Delgado M, Vasoactive intestinal peptide (VIP) and pituitary adenylate cyclase-activating polypeptide (PACAP) as modulators of both innate and adaptive immunity. Crit Rev Oral Biol Med 13, 229–237 (2002). [PubMed: 12090463]
26. Lu B et al. , Abnormalities in monocyte recruitment and cytokine expression in monocyte chemoattractant protein 1-deficient mice. J Exp Med 187, 601–608 (1998). [PubMed: 9463410]
27. Liu XJ et al. , TLR signaling adaptor protein MyD88 in primary sensory neurons contributes to persistent inflammatory and neuropathic pain and neuroinflammation. Sci Rep 6, 28188 (2016). [PubMed: 27312666]
28. Sokol CL, Luster AD, The chemokine system in innate immunity. Cold Spring Harb Perspect Biol 7, (2015).
29. Gschwandtner M, Derler R, Midwood KS, More Than Just Attractive: How CCL2 Influences Myeloid Cell Behavior Beyond Chemotaxis. Front Immunol 10, 2759 (2019). [PubMed: 31921102]
30. Satpathy AT et al. , Zbtb46 expression distinguishes classical dendritic cells and their committed progenitors from other immune lineages. J Exp Med 209, 1135–1152 (2012). [PubMed: 22615127]
31. Caterina MJ et al. , The capsaicin receptor: a heat-activated ion channel in the pain pathway. Nature 389, 816–824 (1997). [PubMed: 9349813]

32. Taylor AM et al. , A microfluidic culture platform for CNS axonal injury, regeneration and transport. Nat Methods 2, 599–605 (2005). [PubMed: 16094385]
33. Huang YL, Walker AS, Miller EW, A Photostable Silicon Rhodamine Platform for Optical Voltage Sensing. J Am Chem Soc 137, 10767–10776 (2015). [PubMed: 26237573]
34. Shumilina E, Huber SM, Lang F, Ca2+ signaling in the regulation of dendritic cell functions. Am J Physiol Cell Physiol 300, C1205–1214 (2011). [PubMed: 21451105]
35. Matzner N et al. , Ion channels modulating mouse dendritic cell functions. J Immunol 181, 6803–6809 (2008). [PubMed: 18981098]
36. Huang E, Showalter L, Xu S, Czernliecki BJ, Koski GK, Calcium mobilizing treatment acts as a co-signal for TLR-mediated induction of Interleukin-12 (IL-12p70) secretion by murine bone marrow-derived dendritic cells. Cell Immunol 314, 26–35 (2017). [PubMed: 28190517]
37. Mootha VK et al. , PGC-1alpha-responsive genes involved in oxidative phosphorylation are coordinately downregulated in human diabetes. Nat Genet 34, 267–273 (2003). [PubMed: 12808457]
38. Subramanian A et al. , Gene set enrichment analysis: a knowledge-based approach for interpreting genome-wide expression profiles. Proc Natl Acad Sci U S A 102, 15545–15550 (2005). [PubMed: 16199517]
39. Liberzon A et al. , The Molecular Signatures Database (MSigDB) hallmark gene set collection. Cell Syst 1, 417–425 (2015). [PubMed: 26771021]
40. Wculek SK, Khouili SC, Priego E, Heras-Murillo I, Sancho D, Metabolic Control of Dendritic Cell Functions: Digesting Information. Front Immunol 10, 775 (2019). [PubMed: 31073300]
41. Franchi L, Eigenbrod T, Munoz-Planillo R, Nunez G, The inflammasome: a caspase-1-activation platform that regulates immune responses and disease pathogenesis. Nat Immunol 10, 241–247 (2009). [PubMed: 19221555]
42. Heng TS, Painter MW, C. Immunological Genome Project, The Immunological Genome Project: networks of gene expression in immune cells. Nat Immunol 9, 1091–1094 (2008). [PubMed: 18800157]
43. Walker CS, Conner AC, Poyner DR, Hay DL, Regulation of signal transduction by calcitonin gene-related peptide receptors. Trends Pharmacol Sci 31, 476–483 (2010). [PubMed: 20633935]
44. Goldsmith ZG, Dhanasekaran DN, G protein regulation of MAPK networks. Oncogene 26, 3122–3142 (2007). [PubMed: 17496911]
45. Perner C, Sokol CL, Protocol for dissection and culture of murine dorsal root ganglia neurons to study neuropeptide release. STAR Protoc 2, 100333 (2021). [PubMed: 33615276]
46. Pinho-Ribeiro FA et al. , Blocking Neuronal Signaling to Immune Cells Treats Streptococcal Invasive Infection. Cell 173, 1083–1097 e1022 (2018). [PubMed: 29754819]
47. Stander S et al. , Expression of vanilloid receptor subtype 1 in cutaneous sensory nerve fibers, mast cells, and epithelial cells of appendage structures. Exp Dermatol 13, 129–139 (2004). [PubMed: 14987252]
48. Zaslona Z et al. , The Induction of Pro-IL-1beta by Lipopolysaccharide Requires Endogenous Prostaglandin E2 Production. J Immunol 198, 3558–3564 (2017). [PubMed: 28298525]
49. Shi C et al. , Bone marrow mesenchymal stem and progenitor cells induce monocyte emigration in response to circulating toll-like receptor ligands. Immunity 34, 590–601 (2011). [PubMed: 21458307]
50. Christensen AD, Haase C, Immunological mechanisms of contact hypersensitivity in mice. APMIS 120, 1–27 (2012). [PubMed: 22151305]
51. Filtjens J et al. , Nociceptive sensory neurons promote CD8 T cell responses to HSV-1 infection. Nat Commun 12, 2936 (2021). [PubMed: 34006861]
52. Liu J, Chen M, Wang X, Calcitonin gene-related peptide inhibits lipopolysaccharide-induced interleukin-12 release from mouse peritoneal macrophages, mediated by the cAMP pathway. Immunology 101, 61–67 (2000). [PubMed: 11012754]
53. Chiu IM et al. , Bacteria activate sensory neurons that modulate pain and inflammation. Nature 501, 52–57 (2013). [PubMed: 23965627]

54. Baral P et al. , Nociceptor sensory neurons suppress neutrophil and gammadelta T cell responses in bacterial lung infections and lethal pneumonia. Nat Med 24, 417–426 (2018). [PubMed: 29505031]
55. Nagashima H et al. , Neuropeptide CGRP Limits Group 2 Innate Lymphoid Cell Responses and Constrains Type 2 Inflammation. Immunity 51, 682–695 e686 (2019). [PubMed: 31353223]
56. Helft J et al. , GM-CSF Mouse Bone Marrow Cultures Comprise a Heterogeneous Population of CD11c(+)MHCII(+) Macrophages and Dendritic Cells. Immunity 42, 1197–1211 (2015). [PubMed: 26084029]
57. Baliu-Pique M, Jusek G, Holzmann B, Neuroimmunological communication via CGRP promotes the development of a regulatory phenotype in TLR4-stimulated macrophages. Eur J Immunol 44, 3708–3716 (2014). [PubMed: 25316186]
58. Liu FL et al. , Interleukin (IL)-23 p19 expression induced by IL-1beta in human fibroblast-like synoviocytes with rheumatoid arthritis via active nuclear factor-kappaB and AP-1 dependent pathway. Rheumatology (Oxford) 46, 1266–1273 (2007). [PubMed: 17569750]
59. Malecka A et al. , Stromal fibroblasts support dendritic cells to maintain IL-23/Th17 responses after exposure to ionizing radiation. J Leukoc Biol 100, 381–389 (2016). [PubMed: 27049023]
60. Chen O, Donnelly CR, Ji RR, Regulation of pain by neuro-immune interactions between macrophages and nociceptor sensory neurons. Curr Opin Neurobiol 62, 17–25 (2020). [PubMed: 31809997]
61. Kupari J et al. , Single cell transcriptomics of primate sensory neurons identifies cell types associated with chronic pain. Nat Commun 12, 1510 (2021). [PubMed: 33686078]
62. Usoskin D et al. , Unbiased classification of sensory neuron types by large-scale single-cell RNA sequencing. Nat Neurosci 18, 145–153 (2015). [PubMed: 25420068]
63. Wang X, Veruki ML, Bukoreshtliev NV, Hartveit E, Gerdes HH, Animal cells connected by nanotubes can be electrically coupled through interposed gap-junction channels. Proc Natl Acad Sci U S A 107, 17194–17199 (2010). [PubMed: 20855598]
64. Ariazi J et al. , Tunneling Nanotubes and Gap Junctions-Their Role in Long-Range Intercellular Communication during Development, Health, and Disease Conditions. Front Mol Neurosci 10, 333 (2017). [PubMed: 29089870]
65. Krummen M et al. , Release of IL-12 by dendritic cells activated by TLR ligation is dependent on MyD88 signaling, whereas TRIF signaling is indispensable for TLR synergy. J Leukoc Biol 88, 189–199 (2010). [PubMed: 20360404]
66. Boes M et al. , T-cell engagement of dendritic cells rapidly rearranges MHC class II transport. Nature 418, 983–988 (2002). [PubMed: 12198548]
67. Nassar MA et al. , Nociceptor-specific gene deletion reveals a major role for Nav1.7 (PN1) in acute and inflammatory pain. Proc Natl Acad Sci U S A 101, 12706–12711 (2004). [PubMed: 15314237]
68. Brasel K, De Smedt T, Smith JL, Maliszewski CR, Generation of murine dendritic cells from flt3-ligand-supplemented bone marrow cultures. Blood 96, 3029–3039 (2000). [PubMed: 11049981]
69. Weischenfeldt J, Porse B, Bone Marrow-Derived Macrophages (BMM): Isolation and Applications. CSH Protoc 2008, pdb prot5080 (2008). [PubMed: 21356739]
70. Katzenell S, Cabrera JR, North BJ, Leib DA, Isolation, Purification, and Culture of Primary Murine Sensory Neurons. Methods Mol Biol 1656, 229–251 (2017). [PubMed: 28808974]
71. Fath T, Ke YD, Gunning P, Gotz J, Ittner LM, Primary support cultures of hippocampal and substantia nigra neurons. Nat Protoc 4, 78–85 (2009). [PubMed: 19131959]
72. Schindelin J et al. , Fiji: an open-source platform for biological-image analysis. Nat Methods 9, 676–682 (2012). [PubMed: 22743772]
73. Chen BC et al. , Lattice light-sheet microscopy: imaging molecules to embryos at high spatiotemporal resolution. Science 346, 1257998 (2014). [PubMed: 25342811]
74. Picelli S et al. , Smart-seq2 for sensitive full-length transcriptome profiling in single cells. Nat Methods 10, 1096–1098 (2013). [PubMed: 24056875]
75. Picelli S et al. , Full-length RNA-seq from single cells using Smart-seq2. Nat Protoc 9, 171–181 (2014). [PubMed: 24385147]

76. Ge SX, Son EW, Yao R, iDEP: an integrated web application for differential expression and pathway analysis of RNA-Seq data. BMC Bioinformatics 19, 534 (2018). [PubMed: 30567491]
77. Inoue H, Nagata N, Koshihara Y, Participation of serotonin in capsaicin-induced mouse ear edema. Jpn J Pharmacol 69, 61–68 (1995). [PubMed: 8847833]
78. Paust S et al. , Critical role for the chemokine receptor CXCR6 in NK cell-mediated antigen-specific memory of haptens and viruses. Nat Immunol 11, 1127–1135 (2010). [PubMed: 20972432]
79. Masuda K et al. , Arid5a controls IL-6 mRNA stability, which contributes to elevation of IL-6 level in vivo. Proc Natl Acad Sci U S A 110, 9409–9414 (2013). [PubMed: 23676272]
80. Foti M et al. , Upon dendritic cell (DC) activation chemokines and chemokine receptor expression are rapidly regulated for recruitment and maintenance of DC at the inflammatory site. Int Immunol 11, 979–986 (1999). [PubMed: 10360972]
81. Sallusto F et al. , Rapid and coordinated switch in chemokine receptor expression during dendritic cell maturation. Eur J Immunol 28, 2760–2769 (1998). [PubMed: 9754563]
82. Graziano VR et al. , CD300lf is the primary physiologic receptor of murine norovirus but not human norovirus. PLoS Pathog 16, e1008242 (2020). [PubMed: 32251490]
83. Choi SC et al. , Cutting edge: mouse CD300f (CMRF-35-like molecule-1) recognizes outer membrane-exposed phosphatidylserine and can promote phagocytosis. J Immunol 187, 3483–3487 (2011). [PubMed: 21865548]
84. Hourcade DE, The role of properdin in the assembly of the alternative pathway C3 convertases of complement. J Biol Chem 281, 2128–2132 (2006). [PubMed: 16301317]
85. Gulati S, Agarwal S, Vasudhev S, Rice PA, Ram S, Properdin is critical for antibody-dependent bactericidal activity against Neisseria gonorrhoeae that recruit C4b-binding protein. J Immunol 188, 3416–3425 (2012). [PubMed: 22368277]
86. Mnich ME et al. , The C-type lectin receptor MGL senses N-acetylgalactosamine on the unique Staphylococcus aureus ST395 wall teichoic acid. Cell Microbiol 21, e13072 (2019). [PubMed: 31219660]
87. Robinson MJ et al. , Dectin-2 is a Syk-coupled pattern recognition receptor crucial for Th17 responses to fungal infection. J Exp Med 206, 2037–2051 (2009). [PubMed: 19703985]
88. Frittoli E et al. , The signaling adaptor Eps8 is an essential actin capping protein for dendritic cell migration. Immunity 35, 388–399 (2011). [PubMed: 21835647]
89. Schmidt F et al. , Flotillin-Dependent Membrane Microdomains Are Required for Functional Phagolysosomes against Fungal Infections. Cell Rep 32, 108017 (2020). [PubMed: 32814035]
90. Mkaddem SB et al. , Lyn and Fyn function as molecular switches that control immunoreceptors to direct homeostasis or inflammation. Nat Commun 8, 246 (2017). [PubMed: 28811476]
91. Huang H et al. , Elimination of GPR146-mediated antiviral function through IRF3/HES1-signalling pathway. Immunology 152, 102–114 (2017). [PubMed: 28464285]
92. Maravillas-Montero JL et al. , Cutting edge: GPR35/CXCR8 is the receptor of the mucosal chemokine CXCL17. J Immunol 194, 29–33 (2015). [PubMed: 25411203]
93. Liao Y et al. , Functional Involvement of Interferon-Inducible Transmembrane Proteins in Antiviral Immunity. Front Microbiol 10, 1097 (2019). [PubMed: 31156602]
94. Ranjbar S, Haridas V, Jasenosky LD, Falvo JV, Goldfeld AE, A Role for IFITM Proteins in Restriction of Mycobacterium tuberculosis Infection. Cell Rep 13, 874–883 (2015). [PubMed: 26565900]
95. Dinarello CA, Overview of the IL-1 family in innate inflammation and acquired immunity. Immunol Rev 281, 8–27 (2018). [PubMed: 29247995]
96. Hurdayal R et al. , Deletion of IL-4 receptor alpha on dendritic cells renders BALB/c mice hypersusceptible to Leishmania major infection. PLoS Pathog 9, e1003699 (2013). [PubMed: 24204259]
97. Saemann MD et al. , Prevention of CD40-triggered dendritic cell maturation and induction of T-cell hyporeactivity by targeting of Janus kinase 3. Am J Transplant 3, 1341–1349 (2003). [PubMed: 14525593]

98. Rivas-Caicedo A et al. , Jak3 is involved in dendritic cell maturation and CCR7-dependent migration. PLoS One 4, e7066 (2009). [PubMed: 19759904]

99. Novoszel P et al. , Psoriatic skin inflammation is promoted by c-Jun/AP-1-dependent CCL2 and IL-23 expression in dendritic cells. EMBO Mol Med 13, e12409 (2021). [PubMed: 33724710]

100. Poggi A, Rubartelli A, Moretta L, Zocchi MR, Expression and function of NKRP1A molecule on human monocytes and dendritic cells. Eur J Immunol 27, 2965–2970 (1997). [PubMed: 9394825]

101. Janssens S, Beyaert R, A universal role for MyD88 in TLR/IL-1R-mediated signaling. Trends Biochem Sci 27, 474–482 (2002). [PubMed: 12217523]

102. Beigel F et al. , Oncostatin M mediates STAT3-dependent intestinal epithelial restitution via increased cell proliferation, decreased apoptosis and upregulation of SERPIN family members. PLoS One 9, e93498 (2014). [PubMed: 24710357]

103. Larrea E et al. , Oncostatin M enhances the antiviral effects of type I interferon and activates immunostimulatory functions in liver epithelial cells. J Virol 83, 3298–3311 (2009). [PubMed: 19158240]

104. Karrich JJet al. , Expression of Plet1 controls interstitial migration of murine small intestinal dendritic cells. Eur J Immunol 49, 290–301 (2019). [PubMed: 30537036]

105. Talukder AH et al. , Phospholipid scramblase 1 regulates Toll-like receptor 9-mediated type I interferon production in plasmacytoid dendritic cells. Cell Res 22, 1129–1139 (2012). [PubMed: 22453241]

106. Tenno M et al. , Essential functions of Runx/Cbfbeta in gut conventional dendritic cells for priming Rorgammat(+) T cells. Life Sci Alliance 3, (2020).

107. Nakamura N et al. , Endosomes are specialized platforms for bacterial sensing and NOD2 signalling. Nature 509, 240–244 (2014). [PubMed: 24695226]

108. Fukao T et al. , Inducible expression of Stat4 in dendritic cells and macrophages and its critical role in innate and adaptive immune responses. J Immunol 166, 4446–4455 (2001). [PubMed: 11254700]

109. Cao W, Tan P, Lee CH, Zhang H, Lu J, A transforming growth factor-beta-induced protein stimulates endocytosis and is up-regulated in immature dendritic cells. Blood 107, 2777–2785 (2006). [PubMed: 16368891]

110. Matic I et al. , Characterization of transglutaminase type II role in dendritic cell differentiation and function. J Leukoc Biol 88, 181–188 (2010). [PubMed: 20371597]

111. Kim JH et al. , Transglutaminase 2 on the surface of dendritic cells is proposed to be involved in dendritic cell-T cell interaction. Cell Immunol 289, 55–62 (2014). [PubMed: 24727157]

112. Wong K et al. , Phosphatidylserine receptor Tim-4 is essential for the maintenance of the homeostatic state of resident peritoneal macrophages. Proc Natl Acad Sci U S A 107, 8712–8717 (2010). [PubMed: 20421466]

113. Dharmadhikari B et al. , CD137L dendritic cells induce potent response against cancer-associated viruses and polarize human CD8(+) T cells to Tc1 phenotype. Cancer Immunol Immunother 67, 893–905 (2018). [PubMed: 29508025]

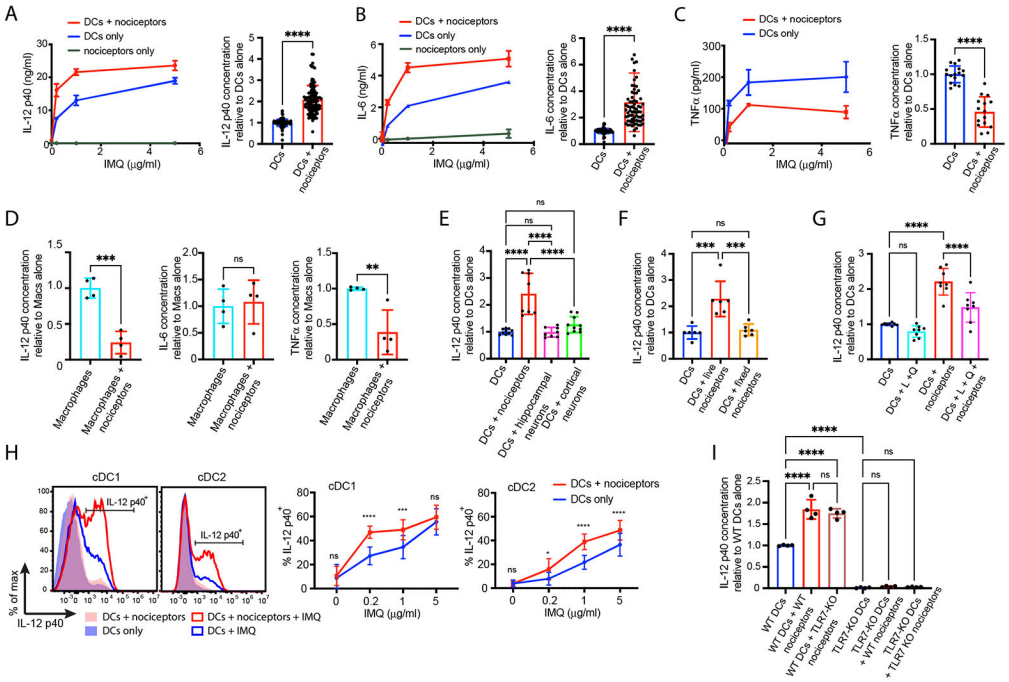

Fig. 1. Nociceptors enhance proinflammatory cytokine production by IMQ-activated DCs in vitro.

BMDCs and nociceptors were either cultured separately or together and treated overnight with proinflammatory stimuli. Indicated cytokines were measured by ELISA in supernatants. (**A-C)** One representative dose response to IMQ (left panels) and summary of (**A)** 42 (n=104), (**B)** 37 (n=74) and (**C)** 7 (n=16) experiments (right panels) for 1 μg/ml IMQ is shown. (**D)** BM-macrophages were cultured alone or in the presence of nociceptors and treated with 1 μg/ml of IMQ overnight. Summary of two experiments (n=4) is shown. (**E)** BMDCs were cocultured with nociceptors, cortical, or hippocampal neurons and treated with 1 μg/ml of IMQ overnight. Summary of three experiments (n=6-10) is shown. (**F)** BMDCs were cocultured with live or fixed nociceptors and treated with 1 μg/ml of IMQ. Summary of three experiments (n=6) is shown. (**G)** DCs were cocultured with nociceptors and treated with lidocaine + QX314 and 1μg/ml IMQ. Summary of four experiments (n=8) is shown. (**H)** Intracellular content of IL-12 p40 in BMDCs left untreated (full histograms) or treated with IMQ (open histograms) in isolation or in a coculture with nociceptors was assessed using flow cytometry. One representative experiment (left) and quantitation of eight independent experiments (right; n=16) is shown. (**I)** WT or *Tlr7*-KO DCs were cocultured with WT or *Tlr7*-KO nociceptors and treated with 1 ug/ml IMQ. Summary of two (n=4) experiments is shown. Across all panels, data represent mean ± s.d. Unpaired *t* test (**A, B, C, and D**), one-way analysis of variance (ANOVA) with Tukey's multiple comparisons test (**F**) or two-way analysis of variance (ANOVA) with Tukey's multiple comparisons test **(E, G, H, and I**) were used for statistical analysis: **P*<0.05, ***P*<0.01, ****P*<0.001, *****P*<0.0001.

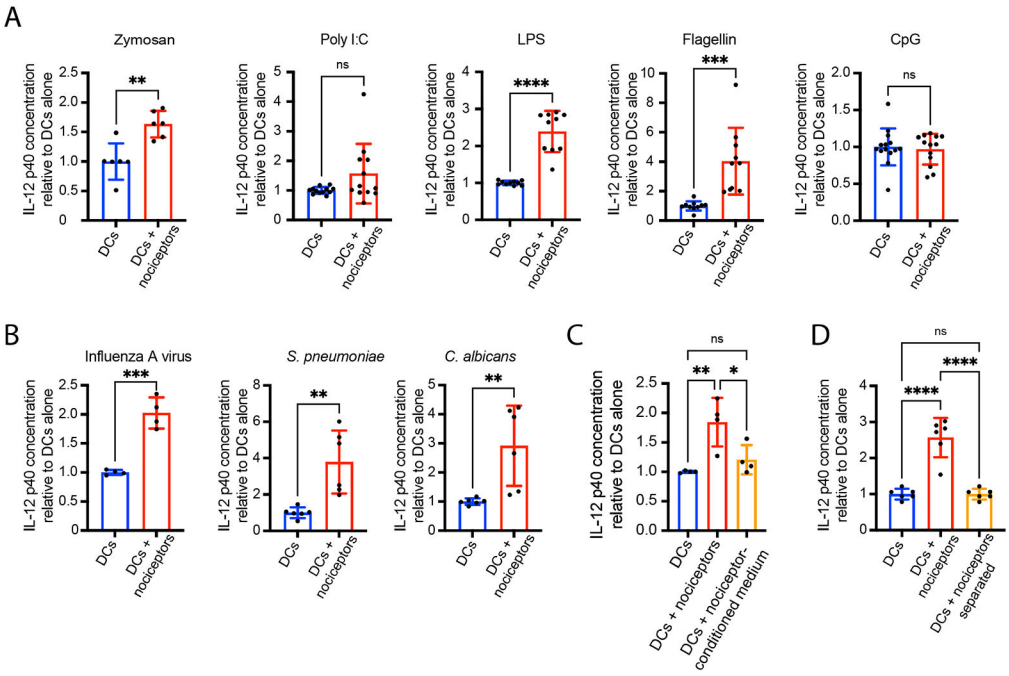

Fig. 2. Nociceptors enhance DC cytokine response to various stimuli in a contact-dependent manner.

BMDCs and nociceptors were either cultured separately or together and treated overnight with indicated (**A)** non-microbial or (**B)** microbial stimuli. Summary of two to five experiments (n=4-12) is shown. (**C)** BMDCs were cultured alone, with nociceptors, or in a transferred medium that nociceptors had been stimulated in and treated with IMQ overnight. Summary of three experiments (n=4) is shown. **(D)** BMDCs were cultured in Transwell plates either alone or with nociceptors in a manner that allowed or prevented direct physical contact between the cell types. Summary of three experiments (n=6) is shown. IL-12 p40 concentration was measured by ELISA in supernatants. Across all panels, data represent mean ± s.d. Unpaired *t* test (**A and B**) or one-way analysis of variance (ANOVA) with Tukey's multiple comparisons test (**C and D**) were used for statistical analysis: **P*<0.05, ***P*<0.01, ****P*<0.001, *****P*<0.0001.

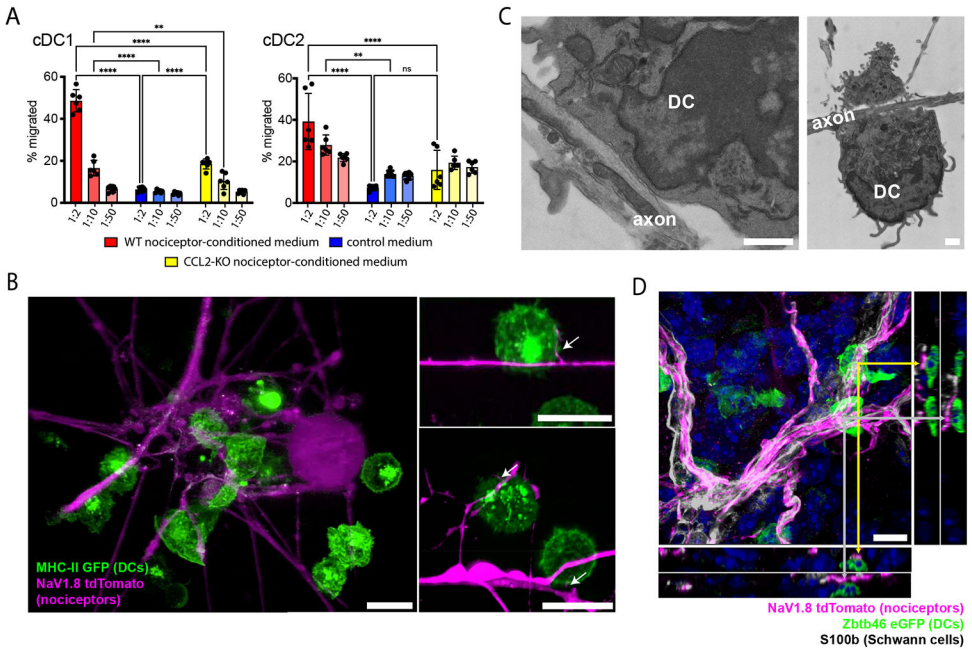

Fig. 3. Nociceptors attract and physically interact with DC in vitro.

(A) Migration of BMDCs toward WT nociceptor-conditioned, control, and *Ccl2*$^{-/-}$ nociceptor-conditioned medium was assessed in a Transwell chemotaxis assay (5-μm pore size). Summary of three experiments (n=6) is shown. Data represent mean ± s.d. Two-way analysis of variance (ANOVA) with Tukey's multiple comparisons test was used for statistical analysis: **P*<0.05, ***P*<0.01, ****P*<0.001, *****P*<0.0001. **(B)** DCs from MHC-II eGFP mice were cocultured with nociceptors from NaV1.8$^{Cre/+}$ ROSA$^{tdTomato/+}$ donors and imaged using a lattice light-sheet microscope (see also movies S2 and S3). Arrowheads highlight some of the points of contact between nociceptors and DCs. Scale bars correspond to 10 μM. **(C)** Transmission electron micrographs of a DC contacting a nociceptor axon. Two representatives of >10 similar images are shown. Scale bars correspond to 1 μM. **(D)** Dermal sheets from bone marrow chimeric animals expressing tdTomato under the NaV1.8 promoter in somatic cells and eGFP under the Zbtb46 promoter in the hematopoietic lineage were stained with anti-S100 antibody to identify Schwann cells and analyzed using confocal microscopy.

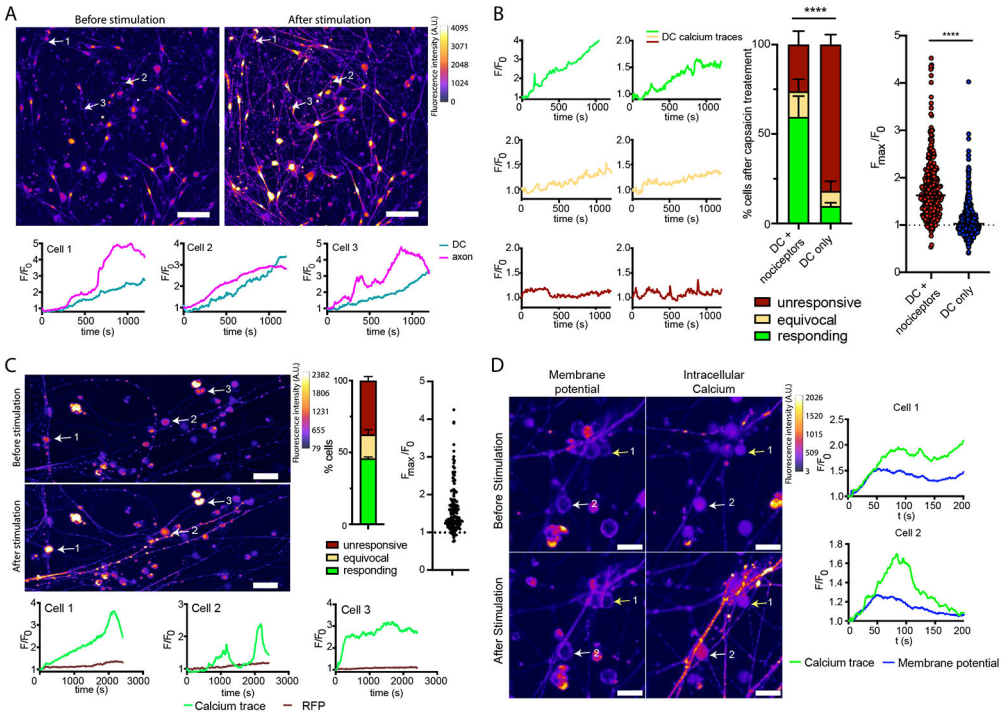

Fig. 4. Activation of nociceptors induces calcium mobilization and membrane depolarization in DCs.

(A) Cells in nociceptor: DC cocultures were loaded with a calcium indicator dye Fluo-4 and imaged on a spinning disk confocal microscope. Left panel shows the culture before and right panel after the addition of capsaicin. Representative calcium traces of DCs and proximal axons (arrowheads) are shown in bottom panels (see also movies S4 and S5). **(B)** Calcium traces of representative responder (green), equivocal (yellow), and unresponsive (dark red) DCs (left panel) and quantification of four independent experiments as shown in Fig. 4A, comparing the proportion of responder cells (middle panel) and the magnitude of calcium response in each cell (right panel) are shown. **(C)** Nociceptors were plated in one compartment (neuronal compartment) of a microfluidic device consisting of two wells that were separated by fluidically-isolated microgrooves. Once neuronal axons had grown across the microgrooves, DCs were added to the second compartment (DC compartment). All cells were loaded with Fluo-4 and the DC compartment was imaged on a spinning disk confocal microscope after capsaicin addition to the neuronal compartment. Some of the responding DCs are highlighted and their calcium traces are shown in the lower panels. One representative and a quantitation of three independent experiments is shown (see also movie S6). **(D)** Cells in a nociceptor–DC coculture were loaded with Fluo-4 and a membrane potential indicator dye (BeRST) and imaged on a spinning disk confocal microscope. Top panels show the culture before and bottom panels after the addition of capsaicin. Some of the responding DCs are highlighted and their calcium and membrane potential traces are shown in the right panel. One representative of two experiments is shown (see also movie S10). Across all imaging panels, warmer colors represent higher intracellular calcium concentration and, in panel D, lower membrane potential (depolarization).

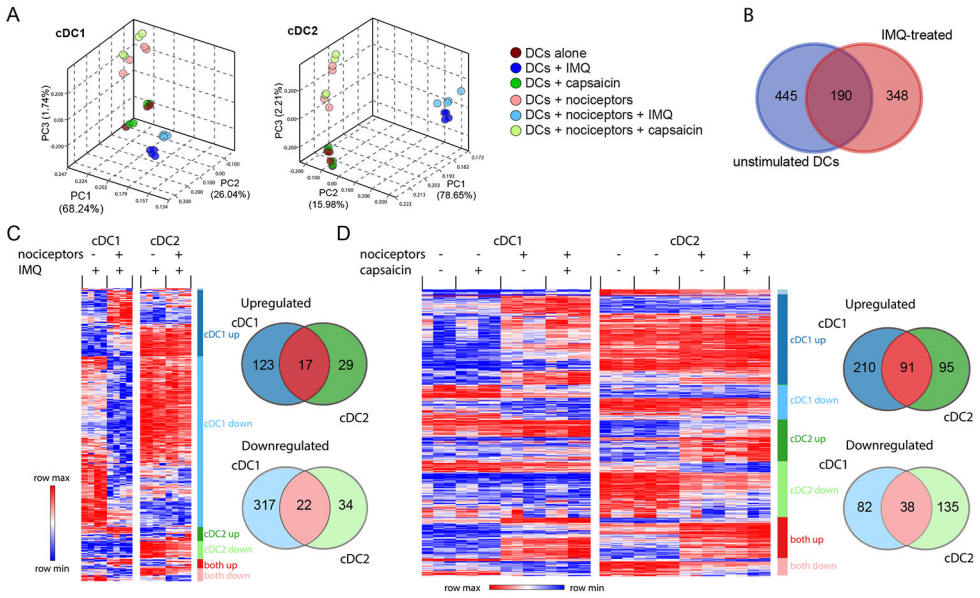

Fig. 5. Nociceptors modulate the DC transcriptome.

(A) Principle component analysis of RNA sequencing data of DCs treated with IMQ or capsaicin in the presence or absence of nociceptors. **(B**) Venn diagram of differentially regulated genes across DC subsets in coculture with nociceptors compared to DC monoculture. (**C and D)** Heatmap of genes differentially regulated (F.C.≥2, FDR 0.1) between (**C)** DCs stimulated with IMQ in monoculture and in coculture with nociceptors or (**D)** DCs left untreated or treated with capsaicin in the presence or absence of nociceptors. Colored bars and sections of the Venn diagrams designate gene-sets that are uniquely differentially regulated in cDC1s (blue), cDC2s (green), or coregulated in the two subsets (red). Darker shades correspond to upregulated genes, lighter shades to downregulated genes.

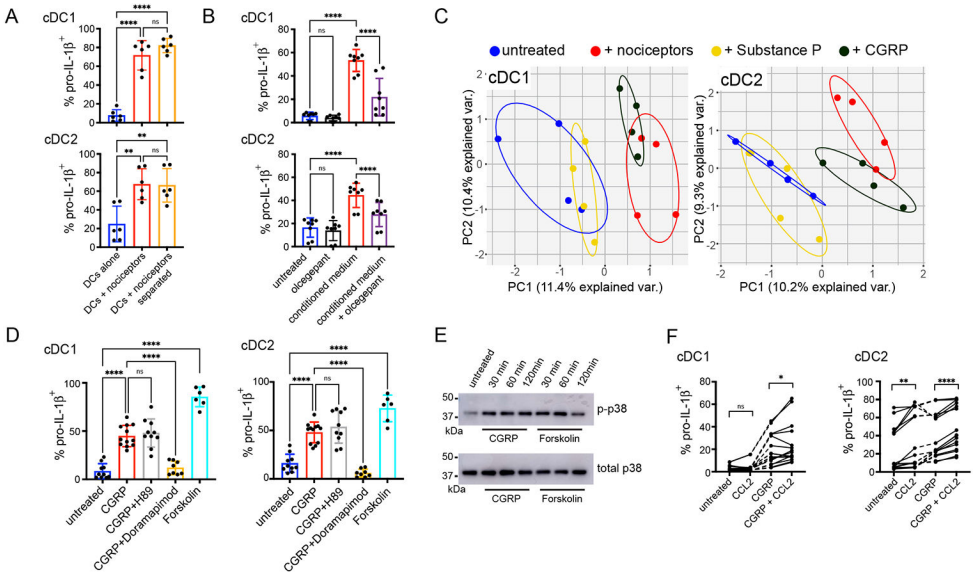

Fig. 6. CGRP induces an enhanced sentinel phenotype in DCs.

Intracellular content of pro-IL-1β was determined by flow cytometry in **(A)** DCs that were directly cocultured with nociceptors, shared medium with nociceptors, or were cultured alone. **(B)** DCs that were incubated with nociceptor-conditioned medium in the presence or absence of CGRP receptor antagonist (olcegepant). Summary of 3-4 independent experiments (n=6-8) is shown. **(C)** Principle component analysis of RNA sequencing data of DCs cultured alone, cocultured with nociceptors or treated with CGRP or Substance P. **(D)** DCs were treated with CGRP, CGRP and dorapamimod (p38 inhibitor), CGRP and H89 (PKA inhibitor), or forskolin (AC activator) overnight. Expression of pro-IL-1β was determined by flow cytometry. A summary of 3-6 experiments per condition is shown (n=6-12). **(E)** DCs were treated with CGRP or forskolin for indicated periods of time and lysed. Phosphorylation status of p38 was assessed by phospho-Thr180/Tyr182-specific antibody in immunoblot analysis (top), total p38 was used as a loading control (bottom). One representative of three independent experiments is shown. **(F)** DCs were plated in wells coated with CCL2 and treated with CGRP overnight. Pro-IL-1β upregulation was assessed by flow cytometry. A summary of eight independent experiments (n=16) is shown. Across all panels, data represent mean ± s.d. One-way analysis of variance (ANOVA) with Tukey's multiple comparisons test **(A)**, two-way analysis of variance (ANOVA) with Tukey's multiple comparisons test **(B and D)**, or paired *t* test **(F)** were used for statistical analysis: **P*<0.05, ***P*<0.01, ****P*<0.001, *****P*<0.0001.

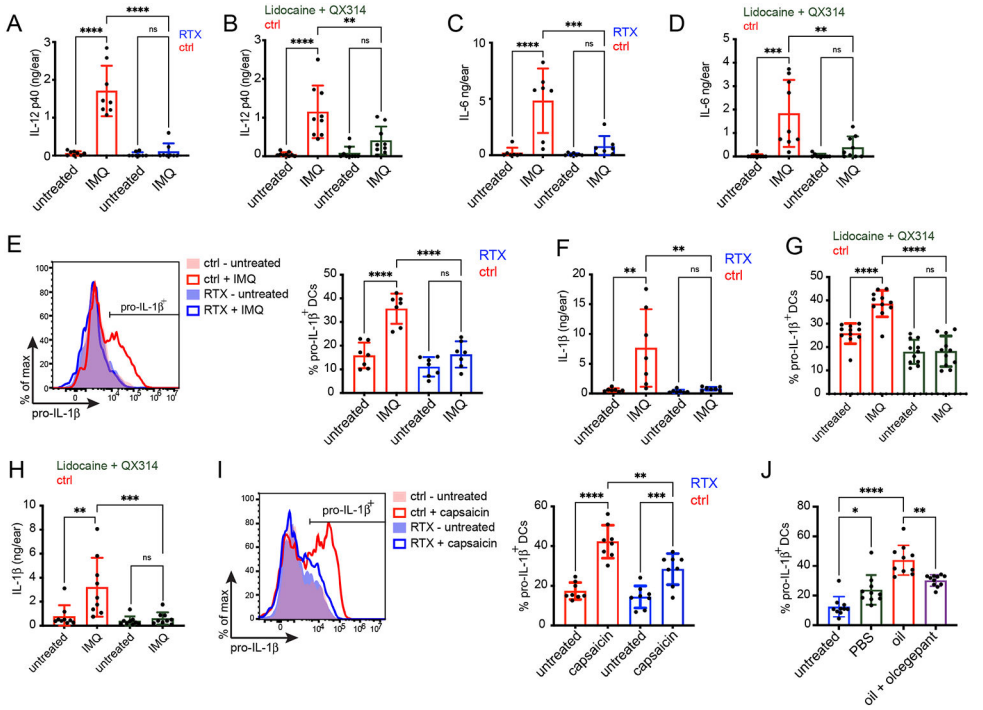

Fig. 7. Nociceptors control DC functions in murine skin in vivo.

(A to D) Ears of mice in which nociceptors had been left intact, were chemically ablated, or were treated with lidocaine + QX314 were then treated topically with IMQ cream. Cytokine accumulation was analyzed by tissue lysate ELISA. Summary of 3-4 experiments (n=7-9 per group) is shown. (**E)** Ears of mice in which nociceptors had been left intact or were chemically ablated were treated with IMQ cream and pro-IL-1β expression by dermal DCs was assessed by flow cytometry. One representative experiment (left) and quantification of three independent experiments (n=7 per group; right) are shown. (**F**) Ears of mice were treated as in (**E**) and accumulation of mature IL-1β cytokine in the tissues was assessed by by tissue lysate ELISA. Summary of three experiments (n=7 per group) is shown. (**G**) Ears of mice in which nociceptors had been left intact, or were treated with lidocaine + QX314 were treated topically with IMQ cream and pro-IL-1β expression by dermal DCs was assessed by flow cytometry. Summary of five experiments (n=11 per group) is shown. (**H**) Ears of mice were treated as in (**G**) and accumulation of mature IL-1β cytokine in the tissues was assessed by by tissue lysate ELISA. Summary of three experiments (n=9 per group) is shown. (**I**) Ears of mice in which nociceptors had been left intact or were chemically ablated were treated with capsaicin and analyzed for pro-IL-1β expression by flow cytometry. One representative experiment (left) and quantification of four independent experiments (n=8 per group; right) are shown. (**J**) Mouse ears were injected intradermally with PBS, oil, or oil supplemented with olcegepant and pro-IL-1β upregulation in DCs was analyzed by flow cytometry 16 hours later. Quantitation of four independent experiments (n=10-11 per group) is shown. Across all panels, data represent mean ± s.d. Two-way analysis of variance (ANOVA) with Tukey's multiple comparisons test was used for statistical analysis: *P<0.05, **P<0.01, ***P<0.001, ****P<0.0001.

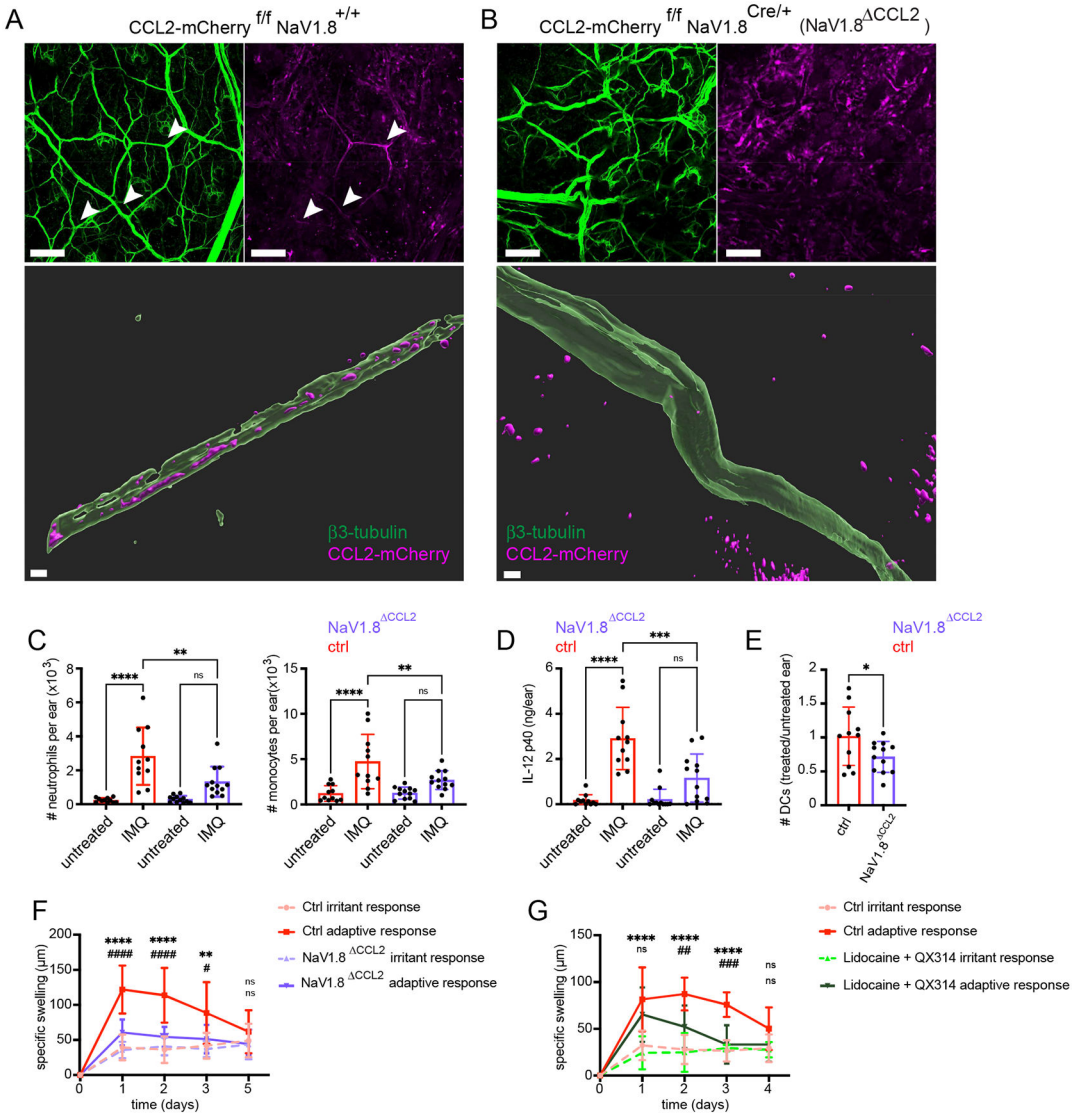

Fig. 8. Nociceptor-derived CCL2 is important for induction of local inflammatory and adaptive immune responses.

Dermal sheets from (**A)** NaV1.8$^{+/+}$ CCL2-mCherry (control) and (**B)** NaV1.8$^{Cre/+}$ CCL2-mCherry (NaV1.8$^{\Delta CCL2}$) animals were fixed, stained with anti-β3-tubulin (green) and anti-mCherry (magenta) antibodies and analyzed using confocal microscopy. Examples of neuronal fibers showing CCL2-mCherry signal are highlighted with arrows (top panels). Surface reconstructions of high-resolution images were performed in Imaris to illustrate the vesicle-like staining pattern of CCL2 (bottom panels). Scale bars correspond to 100 μm (top panels) or 2 μm (bottom panels). **(C** to **E)** Ears of NaV1.8$^{\Delta CCL2}$ or littermate control mice were treated with IMQ cream and (**C)** inflammatory infiltrate, **(D)** IL12-p40 accumulation, and **(E)** ratios of DCs between treated and untreated ears for each animal were analyzed. Summary data of six experiments (n=11-12 per group) is shown. **(F** and **G)** Mice were sensitized with DNFB or treated with vehicle control (acetone) and challenged 5 days later with DNFB on one ear and acetone on the other. Ear thickness was measured at indicated timepoints post challenge and specific swelling was calculated as the difference between

DNFB and vehicle-treated ear for each animal. **(E)** NaV1.8$^{\Delta CCL2}$ or littermate control mice (n=7-8 per group). **(F)** WT mice treated with lidocaine + OX314 prior to, and on two consecutive days after sensitization. All data are presented as mean ± s.d. Two-way analysis of variance (ANOVA) with Tukey's multiple comparisons test was used for statistical analysis. In panels **(F** and **G)** * correspond to statistical comparison between control DNFB-sensitized and control non-sensitized groups, # correspond to statistical comparison between **(F)** control DNFB-sensitized and NaV1.8$^{\Delta CCL2}$ DNFB-sensitized groups, or **(G)** control DNFB-sensitized and lidocaine + QX314 DNFB-sensitized groups. */#P<0.05, **/##P<0.01, ***/###P<0.001, ****/####P<0.001.